Eur. J. Mineral., 34, 603–626, 2022
https://doi.org/10.5194/ejm-34-603-2022

European Journal of Mineralogy
Open Access

ICDP Oman Drilling Project: varitextured gabbros from the dike–gabbro transition within drill core GT3A

Artur Engelhardt[1], **Jürgen Koepke**[1], **Chao Zhang**[2], **Dieter Garbe-Schönberg**[3], **and Ana Patrícia Jesus**[4]

[1]Institute of Mineralogy, Leibniz Universität Hannover, 30167 Hanover, Germany
[2]Department of Geology, Northwest University, Xi'an, 710069, China
[3]Institute of Geosciences, Christian-Albrechts-Universität zu Kiel, 24118 Kiel, Germany
[4]Instituto Dom Luiz, Faculty of Sciences, University of Lisbon, Lisbon, 1649-004, Portugal

Correspondence: Artur Engelhardt (a.engelhardt@mineralogie.uni-hannover.de)

Received: 27 December 2021 – Revised: 30 October 2022 – Accepted: 6 November 2022 – Published: 12 December 2022

Abstract. The Oman ophiolite (Samail massif, Sultanate of Oman) is the largest sub-aerial exposure of oceanic lithosphere on Earth and provides the opportunity to study the accretion and alteration of oceanic lithosphere formed under fast-spreading conditions. Drill hole GT3A (23°06′50.7″ N, 58°12′42.2″ E) of the ICDP (International Continental Scientific Drilling Program) Oman Drilling Project with a length of 400 m aimed at penetrating the dike–gabbro transition of the Samail ophiolite paleocrust in order to shed light on the role of the axial melt lens (AML) during accretion of the lower plutonic crust. AMLs beneath fast-spreading mid-ocean ridges are sandwiched between the sheeted dike complex and the uppermost gabbros and are believed to feed the upper crust and, at least partially, the underlying crystal mush.

Typical gabbroic rocks from dike–gabbro transitions of fast-spreading systems are the so-called "varitextured gabbros", often showing considerable variations in mineral mode, texture and grain size, which are regarded as the frozen fillings of axial melt lenses. Here, we present a detailed petrographic, microanalytical and bulk-chemical investigation of 36 mafic rocks from the drill hole GT3A, which represent mostly varitextured gabbros, revealing a complex formation with several evolution stages. Poikilitic domains formed first, corresponding to an early crystallization stage, where only plagioclase and clinopyroxene of more primitive composition crystallized. Later, domains of granular textures containing also interstitial amphibole and Fe–Ti oxide were formed. This stage is characterized by a magma evolution that underwent crystal fractionation established by lower temperatures due to more efficient hydrothermal cooling at the margin of the AML. A last stage is characterized by pervasive hydrothermal alteration, where all primary minerals have been altered under temperature conditions, varying from the magmatic regime down to greenschist facies. A highlight of this stage is amphiboles showing noticeable compositional zoning. The observation of peculiar microgranular domains, representing relics of stoped exogenic material from the sheeted dike complex, documents the upward migration of an AML in a replenishment event, forcing the AML to burn through previously altered sheeted dikes. This process is responsible for significant assimilation of hydrothermally altered components, indicated by a marked Cl enrichment in the outer zones of magmatic amphiboles. Petrological modeling involving gabbros and basalts revealed that the GT3A rock suite followed a fractional crystallization evolution trend, with a primitive MORB as parental melt with an estimated water content of 0.2 wt % to 0.8 wt %. The modeled liquid lines of descent suggest a magmatic evolution via fractional crystallization, where the basalts correspond to frozen liquids, while the gabbros, especially the more primitive ones, show a significant cumulate component.

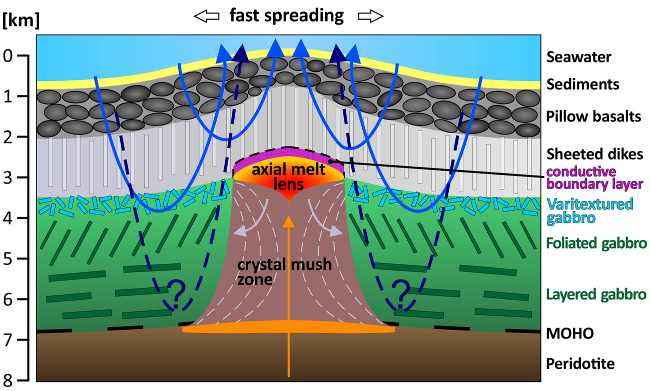

Figure 1. Schematic cross-section of typical fast-spreading oceanic crust showing the location of the axial melt lens (AML) sandwiched between the gabbros and the sheeted dikes (not to scale). The conductive boundary layer typically consists of hornfels (contact-metamorphosed and recrystallized sheeted dike). Blue arrows indicate hydrothermal circulation pathways. Whether a deep hydrothermal circulation exists (dashed blue arrows) is currently under discussion. The orange arrow corresponds to the path of the uprising melt. Dashed white curves in the crystal mush zone show isotherms, and the gray arrows indicate migration paths of crystallized phases. The investigated drill core covers the transition between sheeted dikes and the varitextured gabbros. Modified after Zhang et al. (2014).

1 Introduction

1.1 Role of axial melt lenses at fast-spreading mid-ocean ridges

About two-thirds of the Earth's surface is covered by oceanic crust formed at mid-ocean ridges consisting of basalts in the upper and gabbroic rocks in the lower part. Oceanic crust from fast-spreading ridges is regarded as layered and relatively homogeneous (Canales et al., 2003). Here, seismic experiments revealed the presence of a melt lens sandwiched between the gabbroic sequence and the sheeted dikes, filled nearly with pure melt, often named as the axial melt lens (AML; Fig. 1). The AML resides above a crystal mush zone extending deeply to the crust–mantle boundary (e.g., Detrick et al., 1987; Vera et al., 1990; Sinton and Detrick, 1992).

The role of the AML (Fig. 1) is known to be crucial for the accretion of the crust. Yet, it is not fully understood whether this melt body is the source of the lower gabbroic crust ("gabbro glacier model", e.g., Henstock et al., 1993; Morgan and Chen, 1993; Quick and Denlinger, 1993) or whether it merely supplies the uppermost gabbros and (sub-)volcanic section (see Mock et al., 2021). Other models propose that the lower gabbros originate from in situ crystallization in sills injected into the deep crust ("sheeted sill model", e.g., Bédard et al., 1988; Kelemen et al., 1997). Today, most scientists favor a hybrid model, where both crystal and melt suspension currents originated from the AML together with integrated sill injections (e.g., Boudier et al., 1996; Natland and Dick, 2009; Mock et al., 2021).

The AML is overlain by an impermeable conductive boundary layer (Fig. 1), which separates two convective systems: (1) the AML filled with a basaltic melt at $\sim 1200\,°C$ below and (2) the hydrothermal circulation derived from the entrained seawater, operating at maximum temperatures of 400–500 °C. The conductive boundary layer consists of granoblastic hornfelses, corresponding to former basalts of the sheeted dikes, which were contact-metamorphosed under conditions up to the granulite and two-pyroxene hornfels facies, culminating in anatectic processes expressed by trondhjemitic and tonalitic veins crosscutting the hornfelses. The AML and the overlying conductive boundary layer are transient phenomena, with the potential to move up and down, as a consequence of the magmatic activity beneath the spreading segments (for details see review of Koepke and Zhang, 2021, and references therein).

There are only a few locations worldwide where rocks from the AML horizons have been investigated: the most important are a section of the East Pacific Rise (EPR) crust, drilled by IODP (Integrated Ocean Drilling Program) at Site 1256 in the eastern equatorial Pacific (e.g., Teagle et al., 2012; Zhang et al., 2017; Koepke and Zhang, 2020) and the Samail ophiolite in the Sultanate of Oman (e.g., Macleod and Yaouancq, 2000; Coogan et al., 2002; Müller et al., 2017; France et al., 2021). Typical rocks from such horizons include so-called varitextured gabbros (for definition see next section), which form when the flanks of an AML cool down and crystallize as a result of continued seafloor spreading (e.g., France et al., 2021).

1.2 Varitextured gabbros

The dike–gabbro transition at the Oman ophiolite and from IODP Site 1256 includes heterogeneous, isotropic, often called "varitextured" gabbros, overlying the sequences of "foliated" and "layered" gabbros (Fig. 1). Such gabbros have been interpreted by Macleod and Yaouancq (2000) and Coogan et al. (2002) as a rock suite corresponding to a fossilized AML. They are characterized by heterogeneity in mineral mode, texture and grain size, ranging from fine- to medium-grained on a centimeter scale and therefore often showing a characteristic patchy appearance. Macleod and Yaouancq (2000) suggested that this horizon can be regarded as the end product of highly differentiated MORB melts crystallizing at the margins of an AML. Coogan et al. (2002) and Müller et al. (2017) discovered relics of mineral cores with extremely primitive composition within the relatively evolved varitextured gabbros from the Oman ophiolite. This suggests that during its lifetime, the AML was filled with primitive, parental MORB similar to those observed at the modern EPR (e.g., Wanless and Shaw, 2012). Typical varitextured gabbros from the Oman ophiolite bear magmatic amphibole (e.g., France et al., 2013, 2021; Müller et al., 2017), implying that the related melts were hydrous. Using MELTS modeling (Ghiorso and Sack, 1995), Müller et al. (2017) estimated that water contents for the AML varitextured gabbros from the Wadi Gideah in the Oman ophiolite (Wadi Tayin massif) were between 0.4 wt % and 0.8 wt %.

Varitextured gabbros typically display two major textural domains, often occurring in the same thin section: (1) domains with poikilitic clinopyroxene oikocrysts with dark, spotty appearance enclosing plagioclase chadacrysts, surrounded by (2) domains with typical granular texture of blocky to tabular, sometimes lath-shaped plagioclase, prismatic clinopyroxene and amphibole (e.g., Koepke et al., 2011; Müller et al., 2017; Koepke and Zhang, 2020). As a possible model of formation for varitextured gabbros drilled at EPR Site 1256 by IODP, Koepke et al. (2011) suggested an in situ crystallization scenario, during the cooling and crystallization of an axial melt lens. First, relatively primitive (MORB) melts crystallized the poikilitic domains consisting only of clinopyroxenes enclosing relatively primitive plagioclase, followed by the crystallization of the granular matrix domains with more evolved mineral compositions at lower temperatures. This phase proceeded down to near-solidus conditions, where the interstices have been filled with typical late-stage minerals like amphiboles and oxides.

In this work, we present detailed petrographic, microanalytical and bulk-chemical investigations from varitextured gabbros obtained from hole GT3A of the Oman Drilling Project (details below), which crosscuts the sheeted dike complex down to the uppermost isotropic gabbros (Kelemen et al., 2020). The textures and chemical properties of these gabbros are presently unknown and enable the observation of a fossilized melt lens. The GT3A drill hole was aimed at providing information on the sheeted dike–gabbro transition and on its importance for crustal construction processes and the controls on heat and mass transfer within the uppermost plutonic oceanic crust (Kelemen et al., 2020; France et al., 2021). We aim to quantify the interactions of the magmatic and hydrothermal dynamics that governed at the roof of the AML, which, itself, may cool down to form the suite of the varitextured gabbro, holding information on igneous processes that occurred in the AML. This work focuses on providing a formation scenario of the Oman paleoridge and aims to unfold whether the varitextured gabbros can be regarded merely as the frozen fillings of the AML or rather as cumulate rocks from which magmas were expelled to form dikes and lavas, with their consecutive subsidence forming the lower crust.

2 Geological setting of the Oman ophiolite

The Cretaceous Samail ophiolite, located in the Sultanate of Oman, is the largest sub-aerial exposure of oceanic lithosphere on Earth and shows intact sequences of fast-spreading oceanic crust in many locations. Zircon dating revealed that the paleocrust formed ∼ 95 Myr ago under fast-spreading conditions with a half spreading rate of 50–100 mm a^{-1} (Rioux et al., 2012, 2013). Field relations, in accord with results of geochemical and petrological studies, emphasize a polygenetic origin for the Oman ophiolite (see review in Goodenough et al., 2014, and references therein). The first magmatic phase, generated by decompression melting of the mantle, produced the so-called V1 lavas (Godard et al., 2003, and references therein), with corresponding gabbros resembling the modern EPR in terms of structure, lithology, petrography and bulk crustal thickness. In contrast to the EPR however, the parental melts of the Oman paleoridge show enhanced water contents, owing to the influences of the regional subduction initiation (e.g., Macleod et al., 2013; Guilmette et al., 2018; Belgrano et al., 2019; Koepke et al., 2021; Rioux et al., 2021). A second magmatic phase is based on flux-induced peridotite melting and produced the so-called V2 lava sequence (Godard et al., 2003), which ranges from andesitic to boninitic compositions. The corresponding plutonic rocks in the lower crust and mid-crust are wehrlites, gabbronorites and plagiogranites. In general, rocks produced during the first magmatic stage are intruded by the rocks of the second magmatic phase. These rocks are much more voluminous in the northern part of the ophiolite, whereas the south is dominated by first-magmatic-phase rocks (e.g., Juteau et al., 1988; Goodenough et al., 2014; De Graaff et al., 2019). Therefore, many studies focusing on the understanding of oceanic crust accretion under fast-spreading conditions investigated preferably the southern blocks of the Oman ophiolite. Likewise, our study focuses on the southern blocks of the Oman ophiolite.

The Oman ophiolite was targeted by the multi-national Oman Drilling Project (OmanDP, https://www.omandrilling.ac.uk, last access: November 2022) within the ICDP (International Continental Scientific Drilling Program) to address a diverse range of scientific questions relating to the formation, hydrothermal alteration and weathering of oceanic lithosphere. Drill core GT3A was located at the southern Samail massif in Wadi Abdah (Fig. 2) and intersected a coherent, 400 m long transect through the dike–gabbro transition of the Oman paleocrust with 100 % recovery. The location for the drill hole was carefully selected to be undisturbed by phase-2 magmatism (Koepke et al., 2021) and thus to ensure observations are exclusively related to primary magmatic processes of "normal" fast-spreading ridges (France et al., 2021). The studied area comprises a 20–25° dipping, northeast-southwest-striking dike–gabbro transition zone, which crops out as small hills (e.g., Nicolas et al., 2008; France, 2009; Kelemen et al., 2020). Logged units in hole GT3A consist of basalt, diabase, gabbro, olivine-bearing gabbro, olivine gabbro, disseminated oxide gabbro, diorite, tonalite and trondhjemite. Based on the occurrence of gabbro in the core, Kelemen et al. (2020) divided hole GT3A into four lithologic sequences: (1) an upper dike sequence (0–111.02 m) dominated by basaltic and diaba-

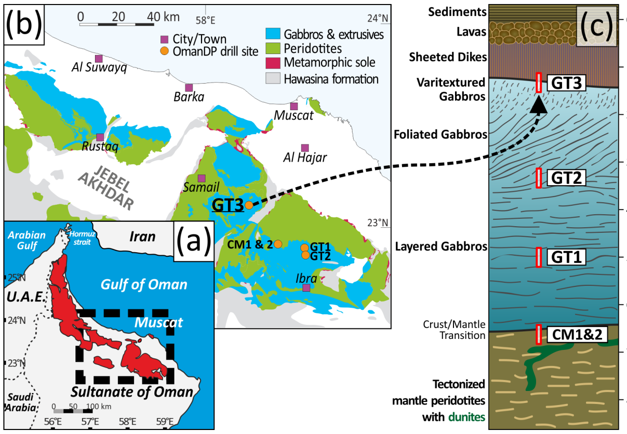

Figure 2. Maps and lithostratigraphic column of the Oman ophiolite. **(a)** Geographical overview. **(b)** Geological map with locations of the OmanDP crustal drill sites. **(c)** Lithostratigraphic sequences of typical oceanic crust formed at fast-spreading ridges including the positions of the OmanDP crustal drill sites. Panels **(b)** and **(c)** modified after Kelemen et al. (2020).

sic dikes; (2) an upper gabbro sequence (111.02–127.89 m) with olivine-bearing and olivine gabbros that intrude and are intruded by basaltic and diabasic dikes; (3) a lower dike sequence (127.89–233.84 m) resembling the first sequence with additional volumetrically minor gabbro in the upper part; and (4) a lower gabbro sequence (233.84–398.21 m) hosting several thick gabbro and oxide gabbro units together with diorite, all intruded by basaltic and diabasic dikes (for more details see Fig. 3 and Kelemen et al., 2020). The crustal thickness of Site GT3 is estimated as $\sim$4.5 km, corresponding to averages from Nicolas and Boudier (2000).

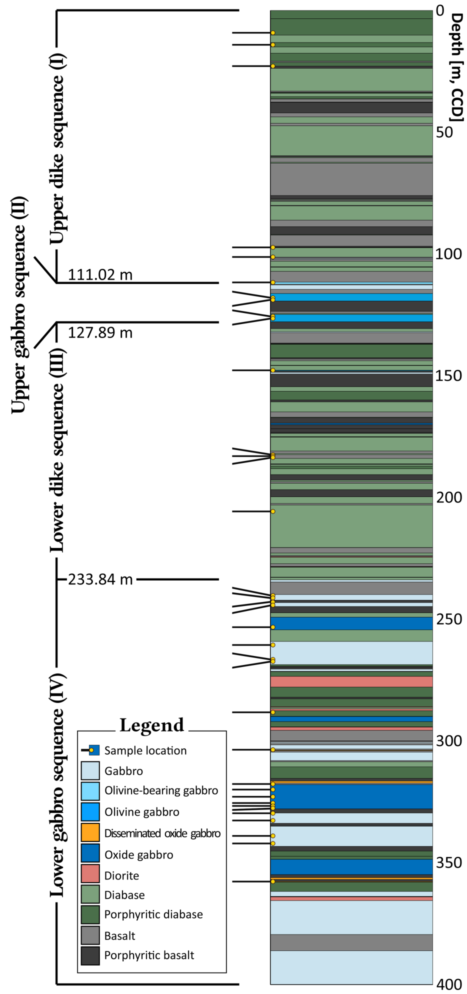

Figure 3. Units and sub-units as defined by Kelemen et al. (2020). The positions of the 36 investigated samples are marked.

3 Methods

3.1 Samples

The petrographic characterization of grain size and lithological classification follow those of Kelemen et al. (2020). In this study we selected 29 samples which could be characterized as varitextured gabbro. Among these are olivine-bearing gabbros, olivine gabbros, disseminated oxide gabbros and oxide gabbros (for rock name definition see method chapter in Kelemen et al., 2020). We also included seven basaltic rocks in our sample suite consisting of basalts with intersertal texture and granular diabases, which have been distinguished by their grain size (Kelemen et al., 2020). Details of the whole sample suite including petrographic features are listed in Table 1. Their location and depth within the GT3A drill core and their assignment to the lithological units and sub-units as defined by Kelemen et al. (2020) are summarized in Fig. 3.

3.2 Analytical methods

Major element compositions for minerals, including F and Cl for amphiboles, have been acquired using a Cameca SX100 electron probe microanalyzer (EPMA), equipped with five spectrometers, $K\alpha$ emission from all elements and an operating system PeakSight at the Institute of Mineralogy, University of Hannover, Germany. The "PAP" matrix correction has been performed after Pouchou and Pichoir (1991). All measurements have been performed with an acceleration potential of 15 kV. For most minerals, a beam current of 15 nA was applied with an acquisition time of 10 s at peak per element. Only for amphibole, a second analysis condition was applied, for the measurement of F and Cl, with a 40 nA beam current and 30 s of acquisition time. The beam size was in general set to 2 µm in diameter.

Bulk rock major element analysis was performed at Activation Laboratories (Actlabs), Canada, via lithium metaborate/tetraborate fusion–inductively coupled plasma (ICP)

Table 1. Samples from the OmanDP drill core GT3A used in this study, including petrographic details.

Sample[a]	Top depth [m]	Lithology[b]	Texture/comment[c]	Grain size[b]	Grain size distribution	Alteration [%]
GT3A-12M-1, 36–41 cm	9.16	plag-phyric basalt	intersertal	cryptocrystalline	bi-modal	85
GT3A-18Z-1, 10–14 cm	13.95	diabase	intergranular	fine-grained	equigranular	90
GT3A-21Z-2, 73–78 cm	22.72	diabase	intergranular	fine- to medium-grained	equigranular	85
GT3A-47Z-4, 64–69 cm	97.27	diabase	intergranular	fine- to medium-grained	bi-modal	60
GT3A-49Z-2, 15–18 cm	101.26	gabbro	varitextured	medium-grained	seriate	90
GT3A-53Z-3, 62–65 cm	111.64	olivine-bearing gabbro	varitextured	medium-grained	equigranular	35
GT3A-55Z-4, 38–43 cm	118.07	olivine-bearing gabbro	varitextured	medium-grained	seriate	25
GT3A-56Z-1, 18–23 cm	118.78	olivine-bearing gabbro	varitextured	medium-grained	seriate	40
GT3A-58Z-2, 32–37 cm	125.71	gabbro	varitextured	medium-grained	seriate	30
GT3A-58Z-3, 43–48 cm	126.46	gabbro	varitextured	medium-grained	seriate	25
GT3A-66Z-3, 54–59 cm	147.83	disseminated oxide gabbro	varitextured	medium-grained	equigranular	55
GT3A-78Z-1, 43–48 cm	182.63	basalt	bears gabbro xenoliths	cryptocrystalline	equigranular	55
		gabbro	xenolith	medium-grained	equigranular	60
GT3A-78Z-2, 33–38 cm	183.08	basalt	bears gabbro xenoliths	cryptocrystalline	equigranular	55
		gabbro	xenolith	medium-grained	equigranular	65
GT3A-78Z-3, 2–7 cm	183.55	basalt	bears gabbro xenoliths	cryptocrystalline	equigranular	65
		gabbro	xenolith	medium-grained	equigranular	55
GT3A-85Z-4, 35–39 cm	205.80	diabase	intergranular	fine-grained	equigranular	55
GT3A-97Z-2, 35–40 cm	240.44	gabbro	varitextured	medium-grained	equigranular	45
GT3A-97Z-3, 43–48 cm	241.38	gabbro	varitextured	medium-grained	equigranular	35
GT3A-98Z-2, 32–37 cm	243.11	gabbro/basalt contact	lithologies show high-T granoblastic overprint to hornfels			
		gabbro	varitextured	medium-grained	seriate	30
		basalt	granoblastic	cryptocrystalline	seriate	90
GT3A-98Z-3, 82–87 cm	244.42	gabbro	varitextured	fine- to medium-grained	seriate	30
GT3A-101Z-3, 46–51 cm	253.31	oxide gabbro	granular	medium-grained	equigranular	85
GT3A-106Z-3, 48–56 cm	260.76	gabbro	varitextured	medium-grained	equigranular	45
GT3A-109Z-2, 48–56 cm	266.78	gabbro	granular	medium-grained	equigranular	50
GT3A-109Z-3, 39–47 cm	267.53	gabbro	varitextured	medium-grained	seriate	30
GT3A-116Z-3, 62–69 cm	288.35	gabbro	varitextured	fine- to medium-grained	seriate	50
GT3A-121Z-4, 18–26 cm	303.86	gabbro/basalt contact				
		gabbro	varitextured	medium-grained	seriate	25
		basalt	intersertal	cryptocrystalline	intersertal	60
GT3A-127Z-2, 68–73 cm	317.96	oxide gabbro	granular	medium-grained	multi-modal	50
GT3A-128Z-1, 34–37 cm	320.14	oxide gabbro	granular	medium-grained	equigranular	50
GT3A-129Z-3, 50–57 cm	325.19	oxide gabbro	varitextured/bears microgranular domains	medium-grained	seriate	25
GT3A-129Z-4, 8–16 cm	325.50	oxide gabbro	varitextured/bears microgranular domains	medium-grained	seriate	25
GT3A-130Z-2, 12–18 cm	326.91	oxide gabbro	varitextured/bears microgranular domains	medium-grained	seriate	40
GT3A-130Z-3, 40–45 cm	327.81	oxide gabbro	varitextured/bears microgranular domains	medium-grained	seriate	35
GT3A-131Z-2, 0–8 cm	329.84	oxide gabbro	granular	medium-grained	multi-modal	45
GT3A-132Z-2, 25–32 cm	332.85	gabbro	varitextured	medium-grained	seriate	35
GT3A-134Z-2, 50–58 cm	339.26	gabbro	varitextured	medium-grained	multi-modal	60
GT3A-135Z-2, 70–78 cm	342.34	gabbro	varitextured	medium- to coarse-grained	multi-modal	30
GT3A-140Z-2, 64–69 cm	357.96	gabbro/basalt contact				
		gabbro	granular	medium-grained	multi-modal	85
		basalt	intersertal	cryptocrystalline	intersertal	75

[a] Hole-core-section, cm top–cm bottom. [b] According to Kelemen et al. (2020, method chapter). [c] The term varitextured includes both poikilitic and granular domains.

analysis with 0.01 % detection limits for major elements except for TiO_2 and MnO, for which the detection limits were improved up to 0.001 %.

Bulk rock trace element analysis has been performed at the Institute of Geosciences of the CAU Kiel University using laser ablation ICP mass spectrometry (LA-ICP-MS) on powder tablets manufactured by wet-milling protocols in aqueous suspension using a planetary ball mill and agate tools (see Garbe-Schönberg and Müller, 2014, for more details). A 193 nm ArF excimer laser ablation system (GeoLasPro Plus, Coherent) coupled to an Agilent 8900cs ICP-MS instrument was used for all measurements. Nano-particulate pressed powder tablets (13 mm in diameter) were inserted into a Zurich-type low-dispersion high-capacity laser ablation cell (LDHCLAC; Fricker et al., 2011) and flushed with 1 L min^{-1} He as the carrier gas. Data acquisition intervals for each laser measurement consist of 20 s background, 40–60 s sample ablation and 20 s monitoring. In order to reduce potential errors caused by surface contamination, every 5–10 s of each data acquisition interval has been discarded via usage of the GLITTER software (for details see Garbe-Schönberg and Müller, 2014). The laser pulse length was adjusted to 17–20 ns with a pulse frequency of 10–15 Hz and an ablation spot size of 80 µm. Reference materials used are JGb-1P (Garbe-Schönberg, 1993; Jochum and Jenner, 1994; Govindaraju, 1995; Imai et al., 1995), BHVO-2P, JB-2P and BIR-1P (Jochum et al., 2016; for more details see Table S3 in the Supplement). In total, bulk rock data were acquired for 23 samples. Bulk rock geochemical data are presented in Table S2.

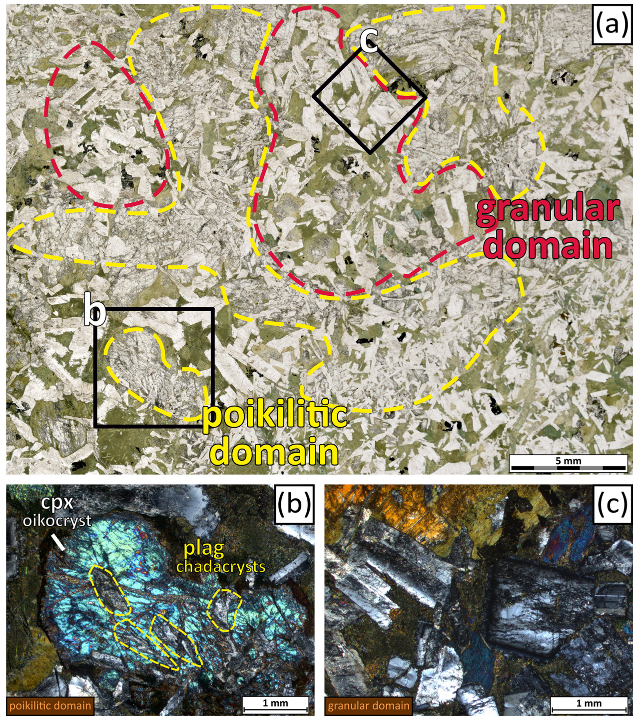

Figure 4. (a) Thin-section photo of varitextured gabbro GT3A-55Z-4, 38–43 cm; plane-polarized light. Poikilitic and granular domains are highlighted. The marked boxes represent details shown in **(b)** and **(c)**. **(b)** Poikilitic texture: lath-shaped plagioclase (plag) chadacrysts are enclosed by clinopyroxene (cpx) oikocrysts; cross-polarized light. **(c)** Granular texture: assemblages of tabular plagioclase and hornblende; cross-polarized light.

4 Results

4.1 Petrographic characterization

The varitextured gabbros of the GT3A drill core are characterized by a wide variability in mineral mode, texture and grain size, ranging from fine- to coarse-grained. The gabbros of our sample set can be classified as olivine-bearing gabbros, gabbros, oxide gabbros and disseminated oxide gabbros (for details see Table 1). Most of the investigated gabbros show two different textural domains: (1) poikilitic domains associated with large, darkish clinopyroxene enclosing plagioclase, resulting in a spotty appearance, and (2) granular domains, identified by blocky to tabular plagioclase, prismatic clinopyroxene and amphibole (e.g., Koepke et al., 2011; Müller et al., 2017; Koepke and Zhang, 2020; also see Fig. 4). Whenever possible, mineral characterization and mineral analyses have been assigned to such textural domains (see Table 1 for petrographic characterization and Table S1 for mineral analyses).

The main primary minerals in the investigated gabbros are plagioclase, clinopyroxene and amphibole. Grain sizes vary from < 0.1 to 10 mm for plagioclases, from < 0.1 to 12 mm for clinopyroxene and from < 0.1 up to 5.5 mm for amphibole. Oxide grains vary in size from 0.2 to 4 mm. Observed mineral modes range from 50 vol %–75 vol % for plagioclase, 20 vol %–40 vol % for clinopyroxene, 2 vol %–10 vol % for amphibole and 1 vol %–5 vol % for oxides. Amphibole occurs as brown relics partially exhibiting euhedral shapes and prismatic habits commonly filling the interstices around plagioclase. Prismatic brown and green amphiboles do coexist side by side or might be zoned; the transition from brown to green occurs mainly gradually or, albeit less commonly, very sharply (see Table S1). A few brown amphiboles exhibit a poikilitic character enclosing oxide grains. Chiefly, green amphibole is replacing clinopyroxene rims, and generally secondary amphiboles prevail in the form of fibrous actinolites. Olivine occurs in three samples as pseudomorphs and is totally altered into fine mixtures of amphibole ± chlorite. Oxides are altered to maghemite, titanite and hematite + rutile (ilmenite). Orthopyroxene has not been observed.

All investigated samples experienced significant and pervasive hydrothermal alteration mostly under amphibolite to greenschist facies conditions, expressed as patches, overgrowths and veins filled with chlorite, epidote, secondary

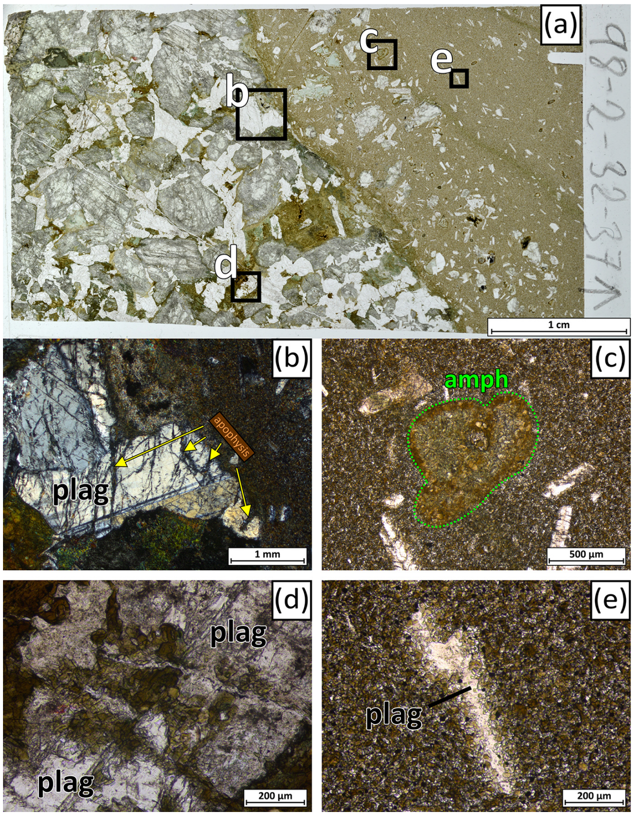

Figure 5. (a) Thin-section photo of sample GT3A-98Z-2, 32–37 cm, showing the contact between a varitextured gabbro and a basalt. Both lithologies show a high-temperature granoblastic overprint due to contact metamorphism resulting from an uprising AML. For details see text. The marked boxes represent details shown in **(b)** to **(e)**; plane-polarized light. **(b)** Apophyses of former basaltic melt penetrating plagioclase of the gabbro at the contact; cross-polarized light. **(c)** Cluster of granoblastic amphibole (amph) replacing former alteration phases; plane-polarized light. **(d, e)** Cluster of amphibole overgrowth as record of high-temperature granoblastic overprint both in the gabbro (infiltrating a plagioclase crystal) and in the basaltic matrix (surrounding a plagioclase xenocryst); plane-polarized light.

amphibole and secondary plagioclase, the latter of which is high in its albite component compared to the primary plagioclase. Clinopyroxene is often pseudomorphically replaced by secondary amphibole, comprising aggregates of pale green actinolite or greenish, sometimes brownish, hornblende.

Thin sections, showing contacts between gabbros and basalts, reveal complex dike–gabbro contact relationships: in thin-section GT3A-98Z-2, 32–37 cm, a wavy, smooth contact between a gabbro and a basalt is visible (Fig. 5a). Apophyses of basalt within minerals of the gabbro (Fig. 5b) clearly indicate that the basalt intruded into the gabbro. During the emplacement of the basalt, the gabbro contact was disintegrated, and some minerals of the gabbro are now visible as xenocrysts within the basaltic matrix directly at the contact

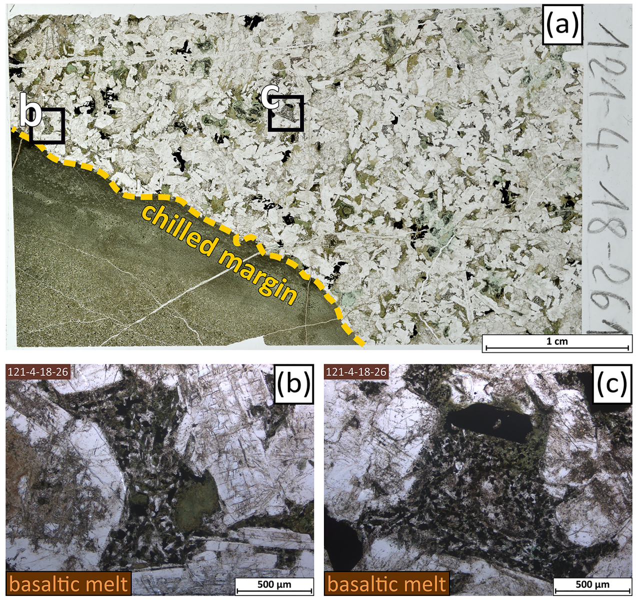

Figure 6. (a) Thin-section photo of sample GT3A-121Z-4, 18–26 cm showing a contact between a varitextured gabbro and a basalt. The basalt at the contact shows a chilled margin, where the basalt coarsens gradually at increasing distance from the margin. **(b–c)** The basalt infiltrated the gabbro expressed by numerous pools of interstitial basaltic melts within the gabbro. All images in plane-polarized light.

(Fig. 5a). Away from the contact, the quantity of xenocrysts decreases, grading within ∼ 1 cm into the normal intersertal texture of the basalt. Some of the observed amphiboles have been converted to aggregates of hornblende and actinolite formed under amphibolite to greenschist facies conditions (Fig. 5c–d).

Another type of intrusive gabbro–basalt contact is visible in Fig. 6, related to sample GT3A-121Z-4, 18–26 cm. Here, the intruding basaltic dike develops a marked chilled margin as demonstrated in Fig. 6a. The basalt infiltrated the gabbro at many places, even ∼ 1 cm away from the contact, as shown in Fig. 6b–c. The difference between this situation and the one previously described is related to differences in the cooling regimes. In the latter case the cooling was faster, forcing the melt to quench to a glassy zone directly at the contact with the relatively low temperature environment of the host gabbro.

In some gabbros we observed rosette-like domains of microgranular assemblages with radiating clinopyroxenes and plagioclases, sometimes associated with interstitial oxides, as shown in Fig. 7. These microgranular assemblages vary in size from 200–1000 µm in diameter and appear to be very similar to those structures observed in the granoblastic hornfelses from IODP hole 1256D, which are interpreted as high-grade metamorphosed, previously hydrothermally altered sheeted dike material along the conductive boundary layer (for details see Koepke et al., 2008). Although

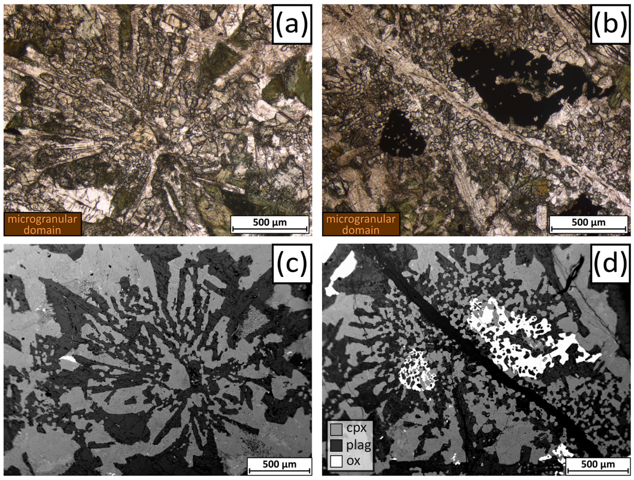

Figure 7. Rosette-like, microgranular domains within two varitextured gabbros (**a, c**: GT3A-129Z-3, 50–57 cm; **b, d**: GT3A-129Z-4, 8–16 cm) consisting of radiating granular clinopyroxenes and lath-shaped plagioclases, sometimes associated with interstitial Fe–Ti oxides **(b, d)**. For details see text. **(a, b)** Microphotographs in plane-polarized light; **(c, d)** backscattered electron images.

we observed such textures in several samples (see Table 1 for details and Table S1 for EPMA analyses), a coherent, decameter-thick layer of granoblastic hornfelses, as observed at IODP Site 1256, was not observed in the GT3A drill core. We discuss consequences of this important observation in Sect. 5.2.

4.2 Mineral analyses

4.2.1 Clinopyroxene

Clinopyroxene compositions show large variations and are different within individual textural domains (Fig. 8). In general, the Mg#'s (Mg# = MgO / (MgO + FeO) · 100, in molar proportions) in poikilitic and granular domains show overlapping values from Mg# 84.5 to 74. The highest Mg# values are recorded in the core areas of clinopyroxene of poikilitic domains with a Mg# of 89, grading down to 74 in the outer core areas. Such high Mg#'s are among the highest values for clinopyroxenes analyzed in the whole gabbro suite of Oman, including gabbros from the mantle transition zone (MTZ) and the base of the gabbroic crust (see Koepke et al., 2022, for a complete Wadi Gideah reference profile), providing evidence for the primitive nature of some melts, which entered the AML. As expected, the Mg#'s from the rim areas are lower, with maximum values of 83. In contrast, the Mg#'s of clinopyroxenes from granular domains have lower values (Fig. 8), varying from 85 to 67, for both cores and rims, whereas microgranular domains lie within the lowermost Mg# of granular clinopyroxene (from 74 to 71). TiO_2 contents are higher in the granular domains (0.13 wt % to 1.12 wt %) compared to the poikilitic domains (0.09 wt % to

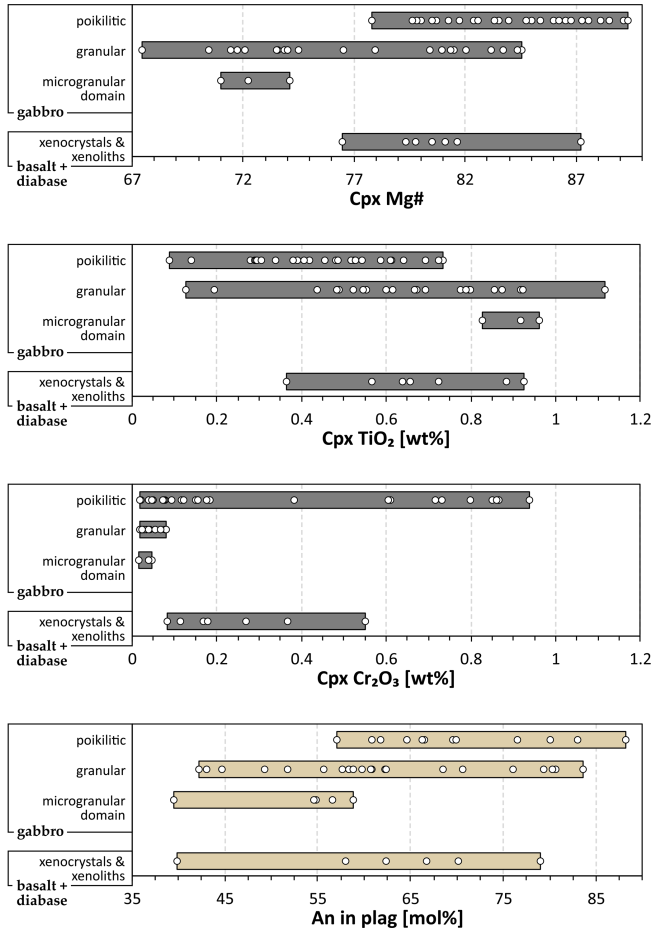

Figure 8. Range of compositions (bars) and averages (white circles) of clinopyroxene and plagioclase recorded in different textural domains. Compositional variation in Mg#, TiO_2 and Cr_2O_3 in clinopyroxene, showing higher values in the poikilitic domains except for TiO_2, which is consistent with the more primitive nature of the poikilitic domains. Clinopyroxenes from microgranular domains show significantly lower Mg#'s. Since the compositional zoning is significantly narrower in clinopyroxenes compared to plagioclase, bars include core measurements. The compositional variation in An contents from core measurements shows higher values in the poikilitic domains overlapping with the granular domains.

0.73 wt %), whereas Cr_2O_3 contents show opposite trends, where the poikilitic domains are elevated (ranging from 0.02 wt % to 0.94 wt %) relative to Cr_2O_3-depleted granular domains (0.02 wt % to 0.08 wt %). Due to the strong overlap between core and rim area values, they are shown combined in Fig. 8. Details can be obtained from Table S1. Clinopyroxene xenocrysts in the basaltic rocks show a similar composition relative to the adjacent gabbros with Mg#'s varying from 87 to 76.

4.2.2 Plagioclase

Plagioclase composition is characterized by a range from primitive to highly evolved compositions with considerable overlap in compositions between the poikilitic and granular domains. The mineral cores of the poikilitic domains range from 88 mol % An down to 20 mol % in the outer rims (Fig. 8). In general, the An content is lower in granular domains, varying from An 83 in the inner core areas down to An 14 in the outer rims. The An contents in plagioclase from the microgranular domains show compositional ranges within the lowermost An interval of granular plagioclase cores between An 60 and An 40. Examples for the compositional variations in plagioclases of both poikilitic and granular domains are shown in Fig. 9. The extreme compositional variations in grains within the individual domains are in strong contrast to the homogeneous plagioclase compositions in the layered and foliated gabbros (VanTongeren et al., 2021; Koepke et al., 2022).

4.2.3 Amphibole

Amphiboles, displaying different colors from deep brown to pale green, also show an extremely broad compositional range. These amphiboles were classified after Locock (2014), using the amphibole nomenclature by the International Mineralogical Association according to Hawthorne et al. (2012). Amphibole often forms poikilitic grains with optical and compositional zoning from brown cores to brownish green rims. The brown cores with elevated concentrations of Al_2O_3, TiO_2 and Na_2O (Fig. 10) are classified as Ti-rich pargasite, Ti-rich magnesio-hastingsite, pargasite, magnesio-hastingsite and magnesio-ferri-hornblende (for more details see Table S1). Crystals with green-brown to green-colored rims show distinctly lower concentrations of Al_2O_3, TiO_2 and Na_2O (Fig. 10) and are classified as magnesio-ferri-hornblende, magnesio-hastingsite and ferro-ferri-hornblende (Table S1). Finally, the zoned crystals are commonly overgrown by pale green aggregates of actinolitic compositions, which are typically low in Al_2O_3, TiO_2 and Na_2O (Fig. 10). Although the analyzed amphiboles show some degree of compositional overlap, there is a clear correlation between color and composition, as demonstrated in Fig 10. Figure 11 shows the relation between tetrahedral Al and Na + K on the A position of the amphiboles, which are both regarded to be dependent on temperature (e.g., Holland and Blundy, 1994), versus the Ti-in-amphibole temperature (more details are discussed in Sect. 5.1). Both parameters of the diagram show a good correlation with the temperature estimates of the Ti-in-amphibole geothermometer.

4.3 Bulk rock geochemistry

Results of bulk major and trace element analyses are summarized in Table S2. Basalts and diabases fall within the total alkali versus silica (TAS) diagram (Le Bas and Streckeisen, 1991) into the discrimination field of basalt (Fig. S1 in the Supplement) with bulk Mg# ranging from 41 to 61 and from 65 to 69, respectively. The gabbros show bulk Mg# from 53 to 80 with olivine-bearing gabbros representing the highest Mg# values. Harker diagrams for Al_2O_3, TiO_2 and Fe_2O_3 displayed in Fig. 14 suggest a more primitive character for olivine gabbros relative to gabbros and oxide gabbros, which show TiO_2 enrichment of up to ~ 2 wt %.

Trace element N-MORB normalized concentrations for GT3A lithologies (Fig. 13) show coherent patterns for fluid-immobile high-field strength elements (HFSE) on the right-hand side of the diagram (plus Th, Nb and Ta), suggesting they are a cogenetic suite. While most HFSE develop relatively flat lying patterns, implying identical relative abundances relative to MORB, Nb and Ta show pronounced negative anomalies, suggesting these elements are depleted in the Oman magmas. Low Nb–Ta in the oxide gabbros can be ascribed to the stronger fractionation of Ta into oxide minerals, thus scavenging this element from the melt (Rollinson, 1993). Abundances for fluid-mobile elements are somewhat more variable, reflecting different degrees of overprint by seawater-derived hydrothermal fluids (Staudigel, 2003) generally decreasing from Cs > Sr > Ba > U > Rb.

Bulk abundances for immobile elements increase from the olivine gabbros, through most gabbros, whereas the oxide gabbros and basalts plot at higher concentrations, within the envelope defined by 1256D gabbros. The moderate positive Eu anomaly and the marked positive Sr anomaly visible in the patterns of all gabbroic rocks could be interpreted as the combined effects of plagioclase accumulation, as it is typical of gabbros in the oceanic crust and results from hydrothermal alteration. Similarly, Zr $\pm$ Hf show increasingly pronounced negative anomalies relative to neighboring rare-earth elements (REE) for olivine gabbros, gabbros and oxide gabbros but are nearly absent in the basalts, indicating preferential fractionation of these elements into the melt fractions.

5 Discussion

5.1 Amphibole evolution: from the magmatic regime to greenschist facies

Fluid–rock interactions play an essential role in mineral genesis during hydrothermal alteration at mid-ocean ridges, potentially regulating heat and mass transfer during the metamorphic evolution of the oceanic crust (e.g., Alt et al., 2010; Currin et al., 2018b; Zihlmann et al., 2018). In order to assess the complex magmatic and metamorphic evolution within this environment, volatile bearing minerals such as amphibole provide pivotal information about thermal and geochemical evolution due to their large range of temperature stability. Indeed, amphiboles are able to record the evolution from a magmatic regime at an early stage of ocean crust

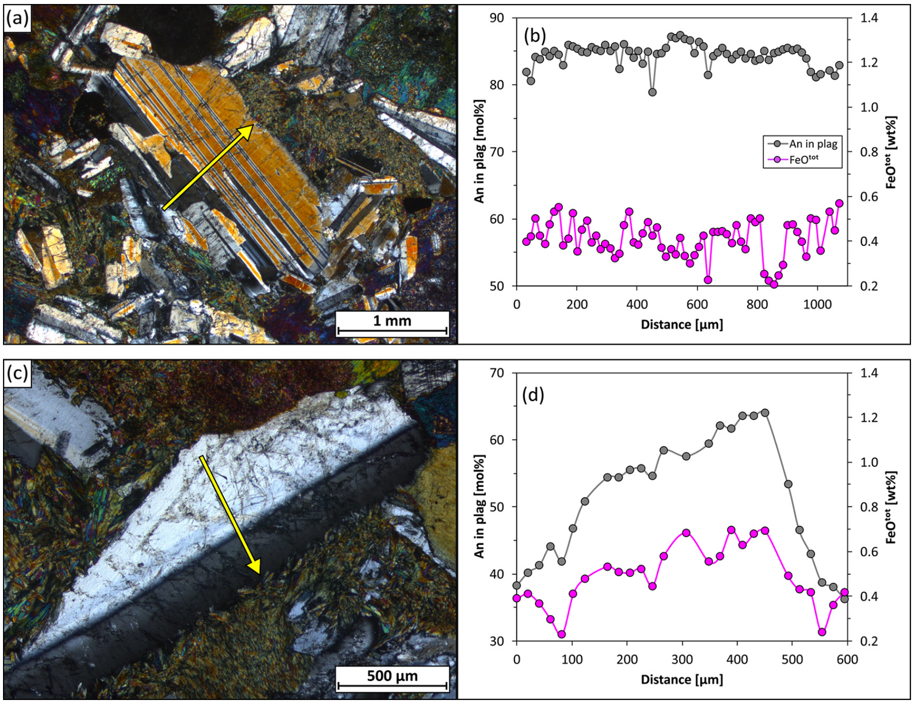

Figure 9. Contrasting compositional features for plagioclases from typical poikilitic (sample GT3A-97Z-2, 35–40 cm; **a, b**) and granular domains (sample GT3A-109Z-3, 39–47 cm; **c, d**). **(a, c)** Microphotograph with plane-polarized light; **(b, d)** EPMA profile for An and FeO content. Plagioclase from poikilitic domains **(a, b)** shows only minor compositional variation with generally higher An contents (up to An 86). In contrast, plagioclases from the granular domain show in general a strong zoning with significantly lower An contents **(c, d)**. The yellow arrows mark the start and end of the EPMA profiles.

formation, as well as throughout a metamorphic stage under amphibolite facies conditions of increased hydrothermal activity, and up to pervasive alteration under (sub-)greenschist facies, which are often accompanied by brittle deformation that leads to a marked amphibole veining (at temperatures above 300 °C; e.g., Coogan et al., 2001; Bosch et al., 2004; Alt et al., 2010; Currin et al., 2018b). Constraints regarding conditions for amphibole formation and distinguishing between magmatic and hydrothermal can be drawn from thermometric constraints. Based on experimental evidence showing that TiO_2 content in calcic amphiboles is strongly dependent on temperature but barely affected by pressure, Ernst and Liu (1998) calibrated the Ti-in-amphibole geothermometer applicable for temperatures between 500 and 1050 °C. Although this geothermometer was characterized by Ernst and Liu (1998) as semiquantitative, the reliability of this geothermometer was validated experimentally (e.g., Koepke et al., 2003; France et al., 2010) and has been used in several studies (France et al., 2009, 2013; Koepke et al., 2008, 2011).

Figure 11 displays the relation between tetrahedral Al and Na + K on the A site of the amphiboles versus the Ti-in-amphibole temperature. Both parameters of the diagram, which are regarded as dependent on the temperature (e.g., Holland and Blundy, 1994), show a good correlation with the temperature estimates of the Ti-in-amphibole geothermometer. Figure 12 demonstrates an example of complex zoning relations, which is representative of many amphiboles in the investigated samples. Typically, the inner brown cores of zoned amphiboles are elevated in Al_2O_3, TiO_2, Na_2O (Fig. 10) and higher Ti-in-amphibole temperatures (800–900 °C) (Ernst and Liu, 1998), implying a magmatic formation (800–900 °C, which is consistent with the estimated temperature). This is further supported by the increased contents of F, implying the importance of a magmatic fluid, since it is assumed that the F content in amphiboles from oceanic gabbros is of magmatic origin (e.g., Coogan et al., 2003). In contrast, lower concentrations of Al_2O_3, TiO_2, Na_2O and the Ti-in-amphibole temperatures are found in the rim areas of the amphibole, implying a formation in the transition between magmatic and metamorphic (hydrothermal) processes formed under amphibolite facies to greenschist facies in the outer rims (550–700 °C, which is also consistent with estimated temperatures). Similar trends are observed in complex zoned amphiboles from other varitextured gabbro samples, providing evidence of the strong influence of seawater-derived fluids during hydrothermal alteration throughout the amphibolite facies overprint.

Since the formation of amphiboles requires high water activities (i.e., mainly water saturation), the wet solidus of gabbros becomes relevant. Formation temperatures above the

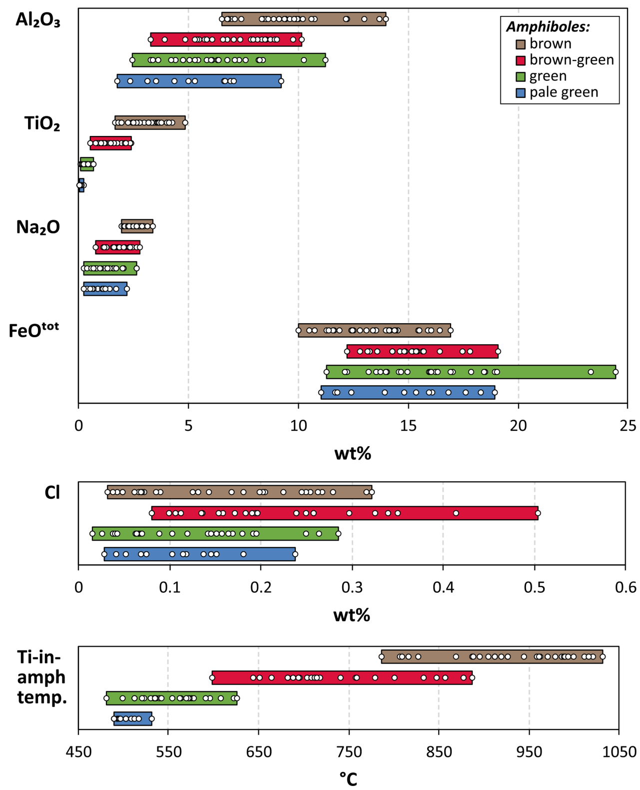

Figure 10. Compositional range (bars) and averages (white circles) for different amphibole groups in varitextured gabbros, classified by mineral color. The concentrations of Al_2O_3, Na_2O, TiO_2 and hence the Ti-in-amphibole temperature range towards lower values from brown via brown-green and green to pale green color of the amphiboles. High TiO_2 contents in the brown amphiboles (up to ~ 5 wt %) reveal a magmatic origin. Relatively high Cl contents (up to 0.5 wt %) imply the presence of a highly saline fluid or brine during formation, interpreted as the result of assimilation of previously hydrothermally altered sheeted dikes (see Discussion).

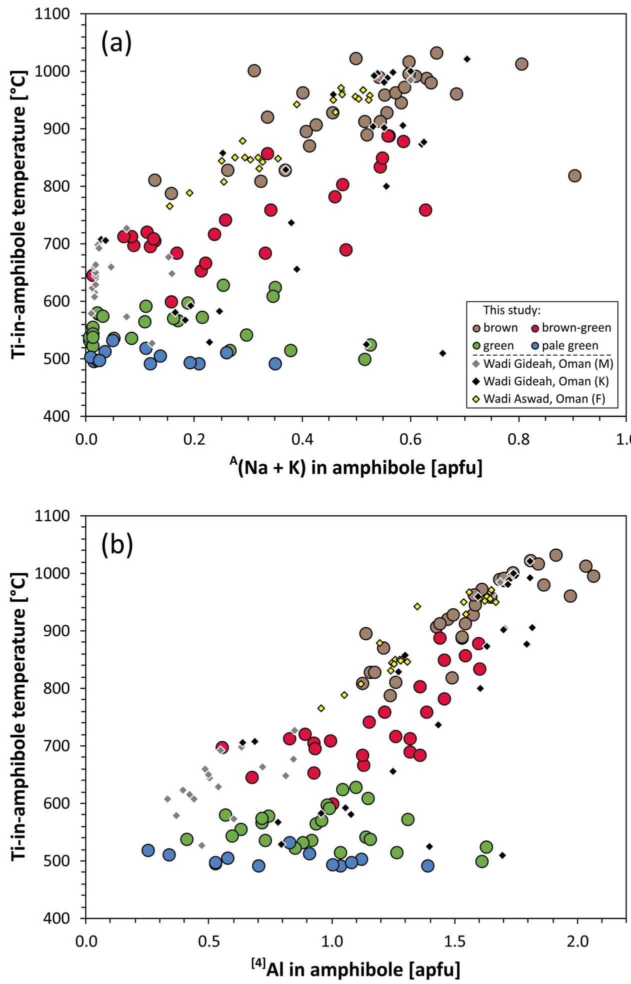

Figure 11. Relationship between tetrahedral Al and Na + K on the A position of the amphiboles versus the Ti-in-amphibole temperature for the different groups, classified by mineral color. Also shown are amphibole data as comparison from other locations of the most southern blocks of the Oman ophiolite: Wadi Gideah (M: Müller et al., 2017, frozen AML; K: Koepke et al., 2022, layered gabbro) and Wadi Aswad (F: France et al., 2021). The amphiboles from the crustal level of a frozen AML show both low tetrahedral Al and ^{A}(Na + K) together with a lower Ti-in-amphibole temperature. In contrast, the layered gabbros from Wadi Gideah exhibit much more scattering, whereas the amphibole data from Wadi Aswad exhibit higher Ti-in-amphibole temperature for tetrahedral Al and ^{A}(Na + K), showing an overlap with the brown and brown-green amphiboles from this study.

hydrous solidus for gabbroic rocks have been estimated to ~ 870 °C for more primitive and ~ 800 °C for evolved gabbros (oxide gabbros; for details see Koepke et al., 2018), resulting in wet solidi of ~ 800 °C for the varitextured gabbros, which are considered relatively evolved (e.g., Fig. 13). This suggests a magmatic origin for those amphiboles with a formation temperature > 800 °C. The Ti-in-amphibole temperatures shown in Figs. 10 and 12 suggest that most of the brown amphiboles could be regarded as magmatic.

Several studies have been performed to shed light on the composition of amphiboles in oceanic gabbros with respect to their formation in three contexts: (1) amphiboles as late-stage minerals in oceanic gabbros from the deeper crust (e.g., Tribuzio et al., 2000; Coogan et al., 2001; Koepke et al., 2005); (2) amphiboles in metamorphic veins of gabbros from the lower crust (e.g., Manning et al., 2000; Currin et al., 2018b; Zihlmann et al., 2018; Zhang et al., 2021); and (3) amphiboles in evolved gabbros from the dike–gabbro transitions, including varitextured gabbros (e.g., Gillis et al., 2003; Koepke et al., 2011; France et al., 2013, 2021; Müller et al., 2017; Zhang et al., 2017). Since the latter topic is the focus of this study, we present in the following a summary on compositions of amphiboles in typical isotropic gabbros from dike–gabbro transitions from the EPR and Oman.

Gillis et al. (2003) used plagioclase–amphibole thermometry that revealed temperatures between 850 and 925 °C.

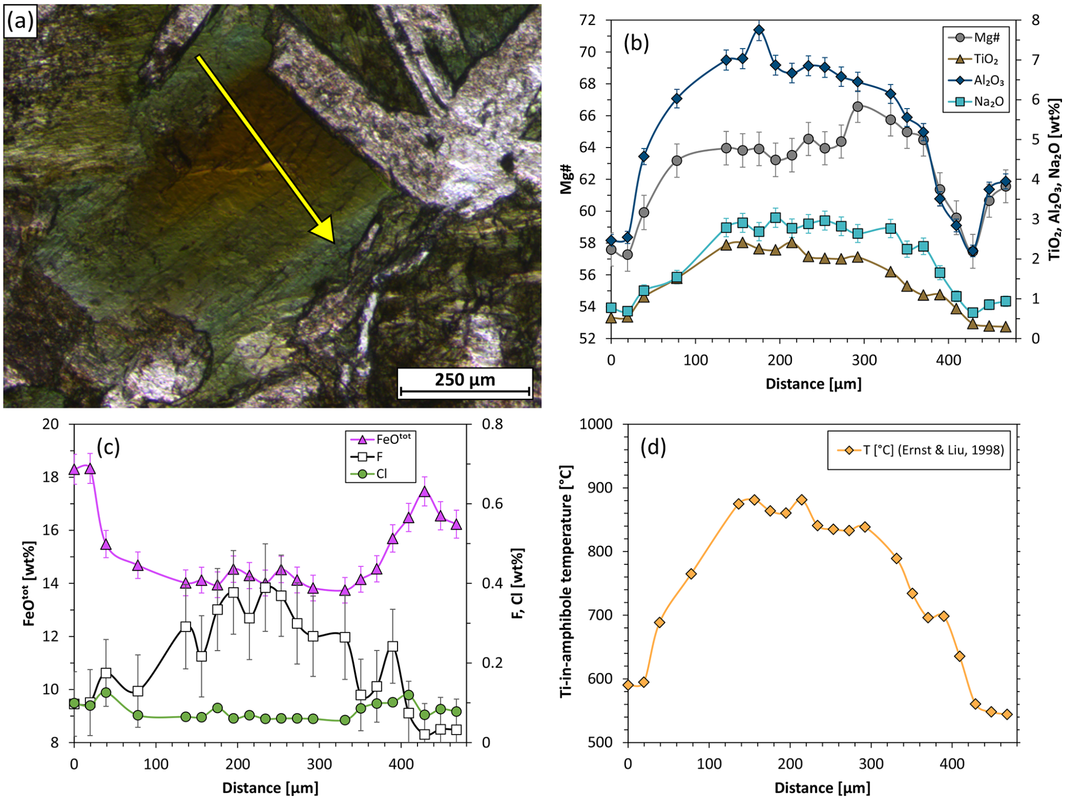

Figure 12. Compositional zoning in an amphibole with a brown core in a typical varitextured gabbro (sample GT3A-109Z-2, 48–56 cm). **(a)** Microphotograph with plane-polarized light with the yellow arrow marking the start and end of the EPMA profile. **(b–d)** Gradual decrease in Mg#, Al_2O_3, Na_2O, TiO_2, F and formation temperature from core to rim. **(c)** Reversed relationship for FeO and Cl. Reported error bars are the count-specific error. Error bars for TiO_2 and Cl are smaller than the symbol size.

France et al. (2013) performed geothermometry on two coarse-grained varitextured gabbros from Wadi Rajimi in the northern massifs of the Oman ophiolite using the semi-quantitative thermometer of Ernst and Liu (1998). They obtained Ti-in-amphibole temperatures for the formation of hornblendes of 780 and 840 °C for the two gabbros. Studies from Koepke et al. (2011) and Zhang et al. (2017) focused mostly on gabbroic rocks from the dike–gabbro transition drilled at IODP Site 1256. In the varitextured gabbros investigated by Koepke et al. (2011), primary magmatic amphiboles occur in typical granular domains of the investigated samples, which are compositionally more evolved compared to poikilitic domains. Thermometry performed on these amphiboles revealed maximum equilibrium temperatures of 925 °C (hornblende–plagioclase equilibrium; Holland and Blundy, 1994) and 1009 °C (Ti-in-amphibole temperature; Ernst and Liu, 1998), which are consistent with a primary magmatic origin. Analyzed magnesio-hastingsitic amphiboles in these gabbros show relatively high Cl contents, between 0.4 wt % and 0.6 wt %, which are significantly higher than expected values for a pure magmatic source (e.g., Coogan et al., 2001; Gillis et al., 2003), implying the involvement of seawater-derived hydrothermal fluids. Due to high Al_2O_3 (up to 13 wt %) and TiO_2 (up to 4 wt %) contents in amphiboles from evolved granular domains of gabbroic rocks from the dike–gabbro transition at IODP Site 1256, Zhang et al. (2017) concluded there was a primary magmatic origin for these amphiboles within these rocks.

The F–Cl amphibole classification proposed by Coogan et al. (2001) provides additional criteria to distinguish between magmatic and metamorphic amphibole formation, based on the contents of the volatiles F and Cl incorporated in the amphiboles, in which high F content generally is regarded as a magmatic signature, while high Cl content implies a metamorphic origin based on interactions with seawater-derived fluids during formation. The classification is based on amphiboles in lower gabbros from the slow-spreading Mid-Atlantic Ridge (MAR), occurring in different structural domains (interstitial late-stage formations, fillings within and replacements of clinopyroxene, vein fillings). Amphiboles from the gabbros of the drill core GT3A define a separate field owing to their high F and Cl concentrations (Fig. 15), implying their formation is different from the four types characterized in Coogan et al. (2001). With high F concentration, indicating a magmatic origin, and high Cl concentration, pointing towards significant influence of seawater-derived hydrother-

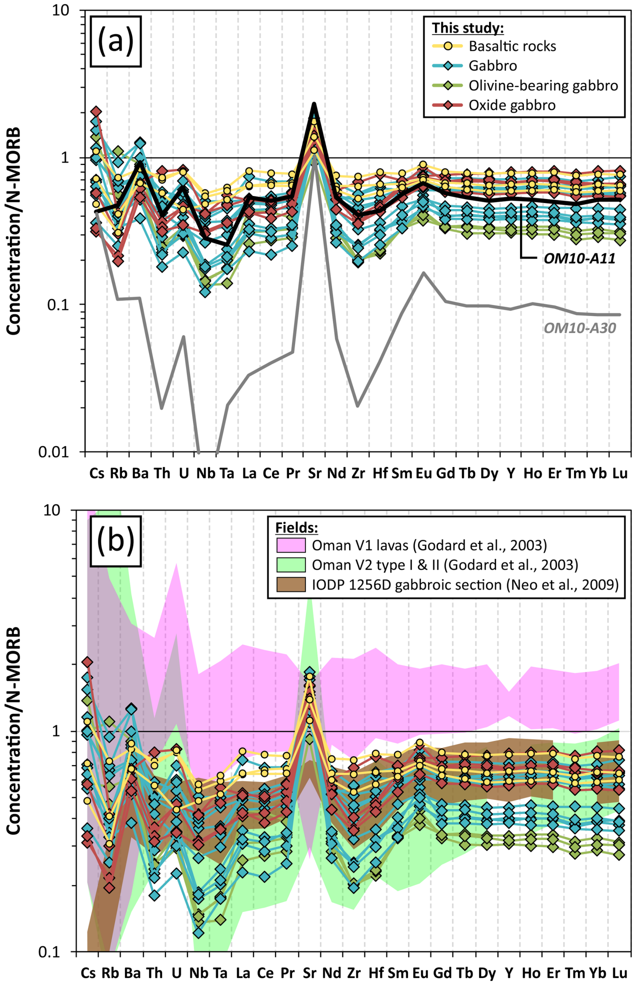

Figure 13. (a) Multi-element diagram (trace element concentration normalized to N-MORB of Gale et al., 2013) for bulk rock compositions from gabbros and basalts from the GT3A drill core. As comparison, rocks from the Oman Wadi Gideah reference transect are included (Garbe-Schönberg et al., 2022). OM10-A11, a primitive basalt from the sheeted dike complex (black line), and OM10-A30, a primitive olivine gabbro of the lower gabbro sequence (gray line). **(b)** Same diagram with a narrower scale. Compositional fields for Oman V1 and V2 lavas (Godard et al., 2003) are included, as well as for gabbros from the IODP core drilled at Site 1256 (Neo et al., 2009).

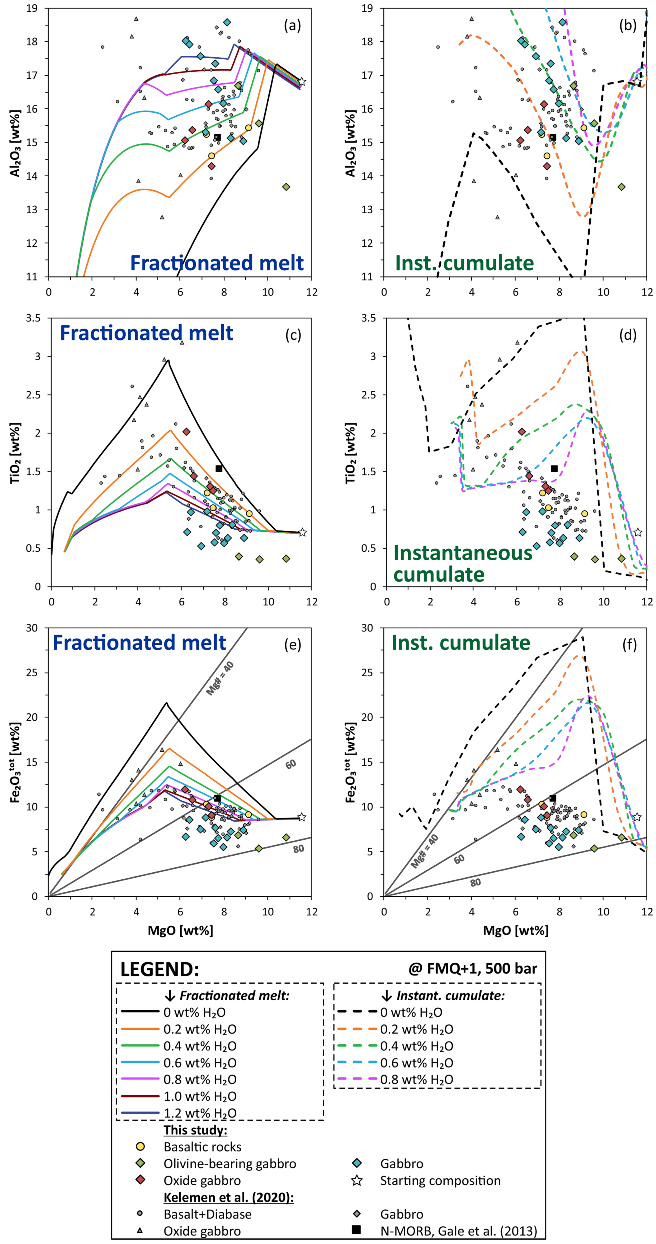

Figure 14. Al_2O_3, TiO_2 and $Fe_2O_3^{tot}$ versus MgO for bulk major element compositions of drill hole GT3A lithologies (data from this study and from Kelemen et al., 2020). **(a, c, e)** Solid lines represent fractional crystallization modeling using MELTS for varying initial H_2O contents. **(b, d, f)** Dashed lines represent the instantaneous cumulate corresponding to the sum of the crystallized phases formed within a temperature interval of 20 °C for different initial H_2O contents. Starting composition is listed in Table 2. For details see text.

mal fluids, GT3A amphiboles include both magmatic and hydrothermal signals in their composition. This seems to represent a characteristic feature for the formation of this type of gabbro in the transition between gabbros and dikes, since amphiboles from evolved, high-level gabbros from similar crustal positions from the EPR and Oman plot into the same area of the diagram (Fig. 15). The reason for this particular feature is very probably that the primary melts, once they reached the AML reservoir and became enriched in the magmatic volatile F, experienced significant contamination, which is further discussed in Sect. 5.2. The brown amphibole cores of magmatic origin (mostly pargasites and hastingsites; see Table S1) are particularly elucidative, since they retained their magmatic F signature, despite a subsequent hydrothermal overprint of the amphiboles, which is a typical feature of the investigated magmatic amphiboles.

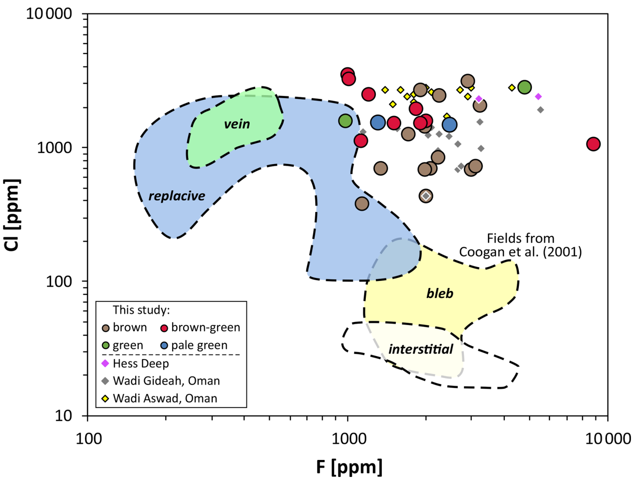

Figure 15. Concentration of F versus Cl in amphiboles from gabbros of the OmanDP drill core GT3A in comparison to those from EPR Hess Deep (Gillis and Meyer, 2001), Oman ophiolite Wadi Gideah (Müller et al., 2017) and Oman ophiolite Wadi Aswad (France et al., 2021). Discrimination fields are from Coogan et al. (2001) for amphiboles related to magmatic (bleb, interstitial) or hydrothermal (vein, replacive) formations. These fields have been evaluated for gabbros from the Mid-Atlantic Ridge. Note that the amphiboles from Oman and those from EPR Hess Deep plot in an area with high Cl and F concentration, not covered by the discrimination fields of Coogan et al. (2001).

Studies on the occurrence of Cl-rich amphibole in low- to high-grade metamorphosed and hydrothermally altered rocks have suggested saline fluids as a general contributor (see Currin et al., 2018a, and references therein). Experimental studies further show that the concentration of Cl in amphiboles can be used to constrain the conditions of the seawater-derived fluids, added to silicate melts. Experimental runs on the addition of Cl from NaCl (4 wt % NaCl; Sato et al., 2005) dissolved in water leads to very small Cl concentrations in amphiboles, e.g., < 0.02 wt % according to Wolff et al. (2013) or < 0.08 wt % according to Sato et al. (2005), showing that the incorporation of Cl is a function of Cl availability. Since many of the investigated brown amphibole cores show significantly higher Cl concentrations (up to 0.32 wt %, Table S1), it is implied that Cl was added to the melt as moderately to highly saline fluid, which is indicated by several experimental studies. Currin et al. (2018a) performed experiments at the transition between hydrothermal and magmatic regimes (up to 900 °C) by adding a saline fluid to the starting material with various Cl contents (up to 50 wt % NaCl) and produced Cl contents in the amphiboles with varying Cl contents up to 0.47 wt %. Moreover, Sato et al. (2005) synthesized amphibole at 3 kbar in a dacitic system with a water-rich fluid moderately enriched in Cl, which yielded Cl content in amphiboles between 0.01 wt % and 0.12 wt %. Cl values from both Sato et al. (2005) and Currin et al. (2018a) (0.01 wt % to 0.12 wt % and 0.02 wt % to 0.48 wt %, respectively) correspond to the number of Cl concentrations analyzed in the cores of the amphiboles of this study (0.03 wt % to 0.32 wt %, Table S1). This further suggests that the melts from which these amphiboles crystallized must have been enriched in Cl. In contrast, extremely Cl-rich amphiboles such as those found in lower crustal oceanic gabbros (up to 5.2 wt %, Currin et al., 2018b) have not been found in the investigated gabbros. The occurrence of such Cl-rich amphiboles is linked to the presence of brines during fluid–rock interaction (Manning and Aranovich, 2014) and has only been found in hydrothermal veins near the transition to the mantle (Zhang et al., 2021).

5.2 Evidence for dike assimilation at the roof of an AML

A characteristic feature of the GT3A varitextured gabbros is the occurrence of microgranular domains: relatively small (< 100, ∼ 60 µm on average) grains of clinopyroxene and plagioclase, often associated with interstitial Fe–Ti oxides, forming a microgranular network (Fig. 7). We found these domains in five samples, from which four samples cluster in a relatively narrow horizon from 325.2 to 327.8 m core depth (Table 1). Here, the microgranular domains are often arranged as rosette-like, roundish structures with radiating clinopyroxenes and plagioclases (Fig. 7a, c). These rosette textural arrangements are identical to quenched structures documented in MORB-type basalts, where rapid crystal growth around cryptocrystalline seed crystals produces radiating, often fan-like clusters of lath-shaped plagioclase and granular clinopyroxene (for details see Koepke et al., 2008). Such structures are typically preserved in the hornfelses formed under granulite or pyroxene hornfels facies conditions at the conducting boundary layer and may survive after stoping in the gabbroic mush of the AML (for details see Koepke et al., 2011). The rosette structures found within the granular domains of the investigated gabbros could thus be regarded as compelling evidence that high-grade metamorphic hornfelses of former basalts of the sheeted dike sequence have been assimilated and integrated into the granular network during gabbro solidification. The relatively evolved compositions of clinopyroxene and plagioclase in the microgranular domains are more in accord with the compositions of the granular than of the poikilitic domains (Fig. 8), implying that the basaltic components have been re-equilibrated under those magmatic conditions, where the granular interstitial network has been solidified.

Very similar domains have been observed in the varitextured gabbros from IODP hole 1256D (EPR, eastern equatorial Pacific) as reported from Koepke et al. (2011). At Site 1256, a part of the dike–gabbro transition of the 15 Myr old EPR crust has been penetrated by drilling, allowing deep insights into the magmatic–metamorphic processes within this peculiar horizon of fast-spreading oceanic crust. In contrast to the GT3A drilling, hole 1256D penetrated a complete, about 70 m thick conductive boundary layer, providing a coherent metamorphic profile of sheeted dikes, starting at the top with (conventionally) hydrothermal alteration in greenschist facies and ending in high-grade metamorphic, microgranular hornfelses, formed under the condition of granulite facies or two-pyroxene hornfels facies (Koepke et al., 2008; Alt et al., 2010). This profile is cut at the bottom by the intrusion of gabbros, from which many show the typical varitextured features (Koepke et al., 2011). The 1256D transect can be regarded as a legacy profile for dike–gabbro transitions from fast-spreading ridges and provides basic knowledge on the metamorphic–magmatic processes in such a horizon: (1) the hornfelses have been formed due to contact metamorphism of the underlying AML and correspond to the conductive boundary separating two convecting systems (hydrothermal circulation above and melt reservoir of the AML below; see review in Koepke and Zhang, 2020); (2) relics of the hornfelses represented as microgranular domains are common in many gabbros below the hornfelses, providing evidence for stoping of the hornfelses during an upward-moving AML after a replenishment event and testifying to the nature of a dynamic AML (e.g., Koepke et al., 2008, 2011); (3) because the hornfelses are dikes that have been hydrothermally altered prior to the high-grade contact metamorphism (Koepke et al., 2008; Alt et al., 2010), the stoping of the hornfelses results in pervasive assimilation, which is expressed by a characteristic Cl enrichment commonly observed in MORBs from fast-spreading ridges (Michael and Schilling, 1989; Fischer et al., 2016; Kendrick, 2019). It is also noteworthy to mention that orthopyroxene, which is a characteristic mineral of the hornfelsic paragenesis recovered from the EPR, was not found in the GT3A gabbros. It is plausible that the hornfelsic relics might have been orthopyroxene-bearing but re-equilibrated under magmatic conditions during the crystallization of the host gabbro, in which orthopyroxene was not stable.

One particular type of microgranular texture observed in the investigated gabbros is the dike–gabbro contact shown in Fig. 5 (sample GT3A-98Z-2, 32–37 cm). Here, both lithologies are overprinted by the same high-grade, granulite-facies metamorphism, resulting in fine-grained hornfelsic textural domains, which is indicated by identical amphibole compositions in both lithologies (see Sect. 4.1 and Table S1). These provide Ti-in-amphibole formation temperatures of 944 and 958 °C (for gabbro and basalt, respectively), implying that the granulite-facies metamorphic overprint event triggered anatectic processes that could have produced those late felsic dikelets consisting of diorite, tonalite and trondhjemite found at many places in the drill core GT3A (Kelemen et al., 2020). The style of overprint in sample GT3A-98Z-2, 32–37 cm (Fig. 5), is quite different in both lithologies, as it is constrained by different kinetics due to the differences in texture and in mineral structures of both protoliths: while the cryptocrystalline basalt shows a complete overgrowth by a microgranular network of amphibole, clinopyroxene, plagioclase and Fe–Ti oxide, very similar to some hornfelses from the IODP drill core 1256D, the much coarser grained gabbro is only partly overprinted, locally showing characteristic domains of microgranular hornfelsic texture with the same mineralogy (Fig. 5d–e). Such domains often correspond to patches and vein-like assemblages, indicating that these locations represent former patches and veins formed by hydrothermal alteration, as was also observed in the hornfelses representing former sheeted dikes from the IODP drill core 1256D (e.g., Koepke et al., 2011). This strongly suggests that gabbros and dikes from the OmanDP GT3A drill core recording granulite-facies contact metamorphism, have been deeply hydrothermally altered prior to the overprint, as it was reported from the IODP drill core 1256D. Later, after the contact metamorphic overprint, both lithologies have been affected by a subsequent hydrothermal alteration stage, which is recorded in the zoning of the amphiboles, indicating conditions of amphibolite facies grading down to greenschist facies.

Microgranular domains representing relics of former granoblastic hornfelses within gabbros of the OmanDP drill core GT3A have also been reported from the core characterization team in the corresponding proceedings (Kelemen et al., 2020). There, these features have been observed in the same interval (323 to 326 m core depth) where we found the microgranular networks. Microgranular domains were also discovered at 243.1 m core depth; therefore we identified a total of two horizons with microgranular domains, providing evidence for processes of stoping and assimilation. Kelemen et al. (2020) systematically investigated the intrusive relationships between individual dikes and gabbros, revealing a very complex intrusion history. Considering the high number of investigated intrusive contacts (more than 230 for the 400 m of drill core) and the fact that each intrusive event destroys most structures formed by previous intrusions, it is indeed highly unlikely to find undisturbed, coherent, decameter-thick metamorphic hornfels profiles, such as the one drilled at IODP Site 1256. Therefore, in a given active ridge segment, only the metamorphic imprints of relatively late replenishment events can be traced by drilling, as was obviously the case at IODP Site 1256.

5.3 Differentiation process within the AML

Mg#'s from basaltic rocks from GT3A and from Wadi Gideah (Fig. 13a, black line) are more primitive than N-MORB (Gale et al., 2013) and show pervasive negative Nb–Ta anomalies. Figure 13 displays the trace element patterns of the GT3A gabbros in comparison to the gabbros of the dike–gabbro transition penetrated by IODP drilling at Site 1256 in the equatorial Pacific, with data obtained by Neo et al. (2009). IODP 1256 gabbros also do not exhibit Nb–Ta anomalies, as would be expected in a typical MORB setting. In fact, both V1 and V2 lavas in Oman show Nb–Ta anomalies (Fig. 13a), emphasizing the formation of the

Oman paleocrust related to a subduction zone environment (e.g., MacLeod et al., 2013; Belgrano and Diamond, 2019). Although the formation of V1 lavas was triggered by decompression melting (Godard et al., 2003), recent work has shown that there were subduction-related contributions during axial magmatism (Belgrano and Diamond, 2019). Concentrations of TiO_2 (0.94 wt % to 1.21 wt %) and Zr (54 to 76 ppm) from basaltic rocks from GT3A are within the range of V1 Geotimes lavas (Belgrano and Diamond, 2019, and references therein). The gabbroic sequence is crosscut by dikes bearing these chilled basaltic rims, emphasizing that the GT3A sequence has likely formed during the first stage of Oman magmatism. Compared to the envelopes defined by Godard et al. (2003), GT3A basaltic rocks show relatively low bulk trace element abundances. One explanation could be related to the fact that these basaltic rocks are quite primitive compared to those studied by Godard et al. (2003) (Mg# ~ 40, whereas for this study we find Mg# 42 to 60) or because GT3A units are transitional to the V2 phase. This hypothesis is in accord with recent work, showing that volcanic units in Oman should not be viewed as isolated magmatic pulses but as continuously evolving (Cravinho et al., 2022).

Excluding fluid-mobile elements (Cs, Ba, U, Sr, Rb), the oxide gabbros and some of the more evolved gabbros show a good correspondence with IODP Site 1256 gabbros, whereas the varitextured gabbros and especially the olivine-bearing gabbros from this study are significantly more depleted. This may indicate that either the parental melts feeding the Oman paleocrust were more primitive or the gabbros from Site 1256 represent a more evolved stage and more primitive components have not been accessed by drilling. However, a stronger cumulate component in GT3A (olivine-bearing) gabbros may also result in the observed decreased trace element abundances due to lower trapped melt fractions, where incompatible elements will concentrate (e.g., Bédard, 1994). This is also the case for the primitive olivine gabbro from the layered gabbro section at Wadi Gideah (Fig. 13a, gray line), in which trace element abundances are vanishingly low. A mild cumulate component in GT3A olivine-bearing gabbros is further supported by stronger positive Eu anomalies found in these rocks, relative to gabbros and oxide gabbros.

In order to evaluate magmatic differentiation processes and to quantify the amount of water in the corresponding melts, we employed an approach using the MELTS algorithm (Ghiorso and Sack, 1995) to model liquid lines of descent (LLDs) with a variation in the meltwater content from 0 wt %–1.2 wt %. Of special interest was evaluating the nature of fractionation, i.e., the relative role of crystal accumulation versus the simple freezing of melts. We chose the same starting composition as MacLeod et al. (2013) and Müller et al. (2017): an experimentally derived MORB parental melt after Kinzler and Grove (1993) with TiO_2 corrections in order to correspond to the special tectonic setting of the Oman paleoridge during a stage of subduction zone initiation (Table 2). To correspond to the crustal level of the AML (dike–gabbro transition), the crystallization pressure was set to isobaric conditions of 50 MPa. As oxygen fugacity (fO_2) we chose slightly oxidizing conditions at FMQ + 1 (FMQ corresponds to the fayalite–magnetite–quartz oxygen buffer). Initial H_2O content was increased stepwise by 0.2 wt % over a temperature interval of 5 °C. The generated plots shown in Fig. 14 refer to the fractionated melt (Fig. 14a, c), and to the instantaneous cumulate (Fig. 14b, d). The instantaneous cumulate refers to the sum of the crystallized phases formed within a temperature interval of 20 °C. For comparison, we included in Fig. 14 the bulk major element data from this study and those from Kelemen et al. (2020) for basalts and gabbros from OmanDP drill core GT3A.

Table 2. Starting composition for modeling with MELTS.

Element	wt %
SiO_2	49
TiO_2	0.7
Al_2O_3	16.8
FeO^{tot}	7.9
MnO	–
MgO	11.6
CaO	11.9
Na_2O	1.92
K_2O	0.05
P_2O_5	–
H_2O	0–1.2
Total	99.87

Starting major element composition after Kinzler and Grove (1993; example 2) with TiO_2 adjustments after MacLeod et al. (2013), which was used for modeling fractional crystallization and crystal accumulation.

The basaltic rocks of this study and those of Kelemen et al. (2020) follow modeled LLDs (TiO_2 and Al_2O_3 versus MgO) for moderately hydrous conditions, revealing initial water contents between 0.2 wt % and 1.0 wt % (Fig. 14a, c), thus being very similar to the results of MacLeod et al. (2013) for the V1 Geotimes lavas, sampled all over the Oman ophiolite. The oxide gabbros follow more or less the modeled LLDs of the basaltic rocks, implying that these can be regarded as frozen melts. Gabbros and olivine gabbros, however, do not follow as a whole the modeled LLDs. In the plot Al_2O_3 versus MgO (Fig. 14a) they form an array crossing the modeled LLDs, and in the plot TiO_2 versus MgO (Fig. 14c) they fall completely outside the field spanned by the LLDs. This clearly shows that these gabbros could not be regarded as frozen melts, implying that these rocks are cumulates or at least bear a significant cumulate component.

This inference is further confirmed by the calculated instantaneous cumulate trends for the olivine-bearing gabbros and gabbros but only for Al_2O_3 versus MgO (Fig. 14b), revealing initial water contents between 0.4 wt % and 0.8 wt %, which is identical to the results derived from the basaltic rocks. In the plot TiO_2 versus MgO (Fig. 14d) and also for Fe_2O_3 versus MgO (Fig. 14f), however, the corresponding data points fall outside the calculated trends for instantaneous cumulate formation. The reason for this mismatch is probably the fact that these rocks do not correspond to a system crystallized under equilibrium conditions, which is a requirement for applying thermodynamic petrological modeling. The presence of both poikilitic and granular domains, which have been formed under different conditions (Fig. 8; see next section), and the strong zoning in the minerals demonstrate a complex formation under disequilibrium. The Al_2O_3-versus-MgO plot is related to phases such as plagioclase, which is an early crystallization product, correctly predicted by the MELTS model (Fig. 14). While plagioclase is linked to the Al_2O_3 content, the MgO content of the diagram is additionally affected by the fractionation of olivine. TiO_2 and Fe_2O_3 are incorporated in early clinopyroxene and further in typical late interstitial minerals like Fe–Ti oxides and amphibole. The latter makes the behavior of these elements problematic to constrain. Another difficulty is the moderate to high grade of alteration observed in the gabbros, affecting changes in mineral compositions by hydrothermal fluxes, which is especially pronounced in mafic phases containing both TiO_2 and Fe_2O_3. To summarize, the petrological modeling reveals complex magmatic formation processes for the gabbroic rocks, with highly evolved constituents (oxide gabbros) representing frozen melts and more primitive ones (olivine-bearing gabbros and gabbros), showing a significant component of cumulate formation.

5.4 Formation of poikilitic and granular textures

A characteristic feature of the studied varitextured gabbros is that the different textural domains contain minerals with significantly different compositions, as demonstrated in Fig. 8. While both plagioclase and clinopyroxene show a wide compositional span (e.g., 70 mol % for plagioclase, Fig. 8), the compositions are clearly more primitive in the poikilitic domains and more evolved in the granular domains. A similar observation was made by Koepke et al. (2011) for varitextured gabbros formed at the EPR, from IODP Site 1256, and by Müller et al. (2017) for varitextured gabbros from the Wadi Gideah in the Oman ophiolite. It should be mentioned that although these authors used the term "subophitic" instead of "poikilitic" as in this study, the described textural domains are virtually identical: large clinopyroxene oikocrysts filled with small plagioclase chadacrysts.

In Fig. 16, An contents in plagioclase versus Mg# in clinopyroxene show that the varitextured gabbros from the GT3A core broadly follow the EPR trends, with two differences: (1) the poikilitic domains from the GT3A core are generally higher both in An content and in Mg#. This may be due to the presence of initial water in the parental melts feeding the Oman paleocrust. A higher water activity produces both higher An contents in plagioclase (e.g., Gaetani et al., 1993; Feig et al., 2006) and higher Mg# values, due to the oxidizing effect of water (e.g., Botcharnikov et al., 2005), which increases the Fe^{3+} species in the melt and thereby shifts the Mg# to higher values. (2) Plagioclase from both domains in the varitextured gabbros from the GT3A drill core shows a much larger range to lower An compositions compared to those from the EPR, implying a stronger grade of differentiation. Also plotted in Fig. 16 are layered and foliated gabbros from the deeper parts of the lower crust from the Wadi Gideah in the Oman ophiolite (Koepke et al., 2022), demonstrating that these gabbros, which are typical cumulate gabbros representing about 4.5 km thickness of the crust (see Fig. 2c), are quite different in composition. They form a relatively narrow array with high An contents in plagioclase and Mg# in clinopyroxene. This also demonstrates the peculiarity of the varitextured gabbros in the horizon of the dike–gabbro transition, which show a significant range of differentiation compared to the gabbros of the lower crust.

It was shown by Koepke et al. (2011) for varitextured gabbros from the EPR at IODP Site 1256 and by Müller et al. (2017) for the Oman ophiolite that some cores of plagioclases and clinopyroxenes of the poikilitic domains contain relics of early crystallization products of very primitive parental melts, which is also true for those varitextured gabbros from the drill core GT3A investigated in this study. Our study provides additional evidence that primitive parental melts are transported through the whole crust directly to the AML, which is also the locus of extensive differentiation from pooled primitive melts. This supports the gabbro glacier model for the accretion of the lower crust, wherein the AML is envisaged as feeding the whole gabbroic crust below the dike–gabbro transition of fast-spreading ridges (e.g., Henstock et al., 1993; see Sect. 1.1) or at least a significant part of it (Maher et al., 2021; Mock et al., 2021).

Based on major and trace elements analysis of plagioclase and clinopyroxene, Koepke et al. (2011) proposed a model for the formation of varitextured gabbros at the dike–gabbro transition of fast-spreading ridges, wherein plagioclase crystallization precedes clinopyroxene in primitive melts transported into the AML, resulting in the formation of poikilitic clusters. The main magmatic process is in situ fractionation, where the fractionated melt stays in place within a crystal mush, which is cooling, presumably due to the proximity of the AML's margins. These are affected by hydrothermal circulation, enabling the removal of the latent heat of crystallization. After the formation of the poikilitic clusters, the degree of crystallization increases, resulting in the formation of a connected framework around the poikilitic domains, consisting of clinopyroxene and plagioclase showing a more evolved composition, followed by interstitial amphiboles and

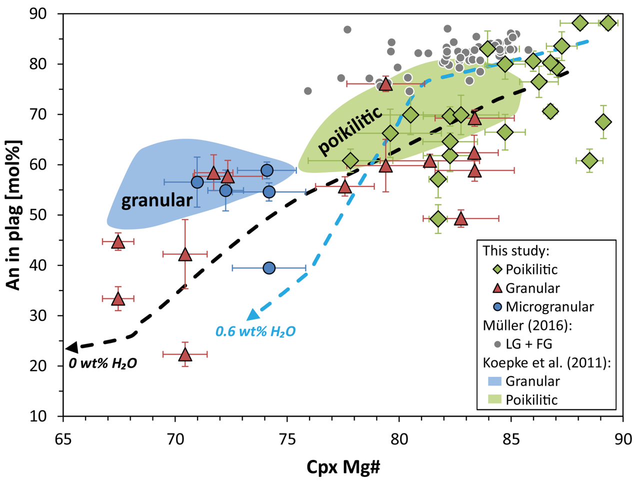

Figure 16. Sample averages of An content in plagioclase versus Mg# in clinopyroxene evolution trends for varitextured gabbros from the GT3A drill core, shown for the different textural domains (poikilitic, granular, microgranular). Green and blue fields define poikilitic and granular domains from varitextured gabbros from IODP hole 1256D (EPR, from Koepke et al., 2011). The data of the GT3A drill core show a similar correlation to those from the EPR but with generally higher An contents, which is due to the hydrous nature of the Oman parental melts. Data from typical layered and foliated gabbro from the lower gabbroic crust of the Oman ophiolite (Wadi Gideah; Müller, 2016) are also included, spanning a compositional field which is significantly different compared to the varitextured gabbros from the dike–gabbro transition. The black and the blue arrows correspond to evolution trends modeled for fractional crystallization with MELTS for 0 wt % and 0.6 wt % initial H_2O. From this, it is obvious that at least the start of differentiation recorded in the poikilitic domains proceeded at high water activities. Error bars are the 1σ standard deviation for clinopyroxene Mg# and plagioclase An content.

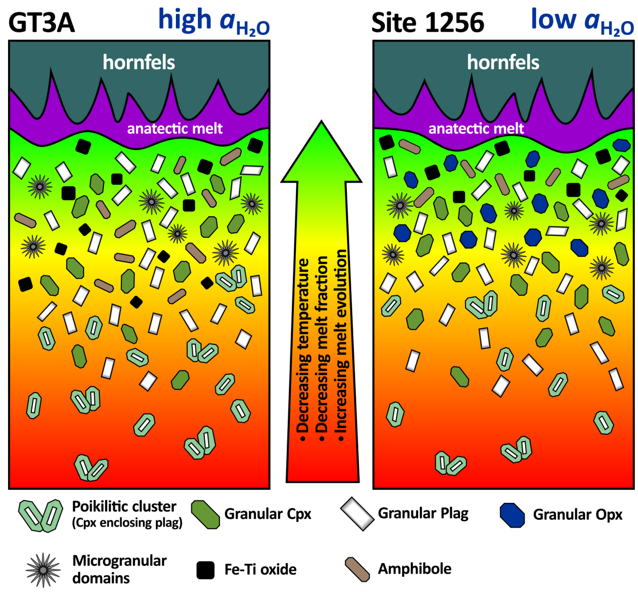

Figure 17. Schematic sketch of a cross-axis view illustrating the upper part of the AML near the conductive boundary layer for the crystallization progress of the Oman GT3A lithologies (left) compared to the drilled core at IODP Site 1256 from the EPR (right). In the early stage of crystallization, both sites show sporadically poikilitic clusters followed by granular plagioclase and granular clinopyroxene. Olivine may join these assemblages at both sides, not shown in this sketch. Owing to the higher water activity in the GT3A system, here amphibole together with Fe–Ti oxides crystallized significantly earlier compared to Site 1256. The microgranular domains, recorded from both sites, correspond to relics of stoped dike material from the AML roof. The crystallization of (late) orthopyroxene is restricted to the EPR site. For details see text.

Fe–Ti oxides. This process is manifested in the formation of the granular domains. Considering the marked similarities of the studied varitextured gabbros with those from the EPR at IODP Site 1256, we assume a very similar formation. One characteristic difference between these two sites is the lack of orthopyroxene in the granular domains of the gabbros from the GT3A drill core. We attribute this to a higher water activity prevailing in the AML of the Oman paleoridge, as a consequence of the tectonic setting in the environment of subduction zone initiation. High water activities stabilize the formation of early amphibole (e.g., Pichavant and Macdonald, 2007), which is, together with clinopyroxene, the dominant mafic phase in the varitextured gabbros of the GT3A drill core. Moreover, a high water activity has the potential to destabilize orthopyroxene (Feig et al., 2006), which is obviously the reason for the general lack of orthopyroxene in the gabbros of the Oman dike–gabbro transition. Furthermore, a high water activity results in more oxidizing conditions, which in turn stabilizes Fe–Ti oxides, as demonstrated by experimental studies (e.g., Toplis and Carroll, 2005; Koepke et al., 2018). This is probably the reason for the relatively common occurrence of oxide gabbros in the GT3A drill core of the Oman ophiolite (Kelemen et al., 2020), in contrast to IODP Site 1256.

5.5 Magmatic processes at the roof of an AML – a formation scenario for the Oman paleoridge

Taking all analytical results and petrographic observations into account, we suggest the following formation scenario for the varitextured gabbro from the GT3A core drilled in the Wadi Abdah within a dynamic AML system, characterized by a rising stage after replenishment and a subsequent cooling stage due to hydrothermal circulation. This is based on previous work on the genesis of varitextured gabbro from the EPR and Oman ophiolite (Koepke et al., 2011; Müller et al., 2017), accordingly adapted in terms of the special observations related to the GT3A drill core and demonstrated in Fig. 17.

Stage 1, $t = t_0$. After a replenishment event, the AML migrates upward, establishing a new steady state at a relatively high position. During the upward migration, the AML burns through previously altered sheeted dikes, resulting in stoping processes and assimilation of hydrothermally altered, exogenic roof material, which increases the water content in the melt and adds seawater-derived fluid-mobile elements like Cl.

Stage 2, $t = t_1$. The rising of the AML stops in a high position, transforming the overlying previous hydrothermally altered sheeted dikes to granoblastic hornfelses by intense contact metamorphism (formation of a conductive boundary layer), with local partial melting of the roof rocks leading to felsic veins (Erdmann et al., 2017). At this stage, stoped parts of the AML roof representing granoblastic hornfelses sink into the melt and form those relics, which can be observed in the GT3A gabbros as microgranular domains. Cooling of the melts starts due to the loss of heat supply from below after the replenishment is finished in combination with convective cooling from above by seawater-derived hydrothermal circulation.

Stage 3, $t = t_2$. As a consequence of cooling, the AML starts to freeze at the roof and margins by crystallizing plagioclase followed by clinopyroxene, which encloses the plagioclase crystals and forms relatively primitive poikilitic clusters. At places where the melt is more primitive, olivine crystallizes first, as is evident from some olivine pseudomorphs observed in olivine-bearing gabbros among the varitextured gabbros. These early phases have the potential to cluster and accumulate, leading to the specific cumulate character suggested from the MELTS modeling.

Stage 4, $t = t_3$. Finally, the melt surrounding the poikilitic cluster, which is meanwhile more evolved due to the crystallization of early phases, freezes to a more evolved granular network, consisting of tabular plagioclase and prismatic clinopyroxene, subsequently followed by Cl-enriched amphiboles and Fe–Ti oxides. The crystallization of the latter phases is forced by the high water activity (which in turn also increases fO_2). The crystallization of the granular network proceeds under marked disequilibrium conditions, as evidenced by the extreme zoning observed especially in plagioclase (Fig. 9) and amphibole (Fig. 12).

Stage 5, $t = t_4$. The magmatic stage merges more or less continuously into a high-temperature metamorphic stage, as evidenced by coherent amphibole zoning revealing Ti-in-amphibole formation temperatures shifting from the magmatic into the metamorphic regime (Fig. 11). Further cooling under the presence of hydrothermal fluids leads to mineral formation in the amphibolite facies, followed by the greenschist facies and finally down to the sub-greenschist facies (zeolite + prehnite + carbonates); the latter is often accompanied by brittle deformation, leading to a marked veining and formation of low-temperature alteration phases.

Following such an evolution sequence and still in a stage of intense hydrothermal cooling at low temperatures, dikes of basaltic material may intrude again, originating from a (new) AML located significantly deeper and leading to the typical microcrystalline basaltic textures often with the chilled margins at the contact seen in GT3A core (Fig. 6; Kelemen et al., 2020). Another scenario could be that the whole sequence is subsequently intruded by a new AML, which may rise up after a new event of replenishment, reproducing the magmatic–metamorphic sequence outlined above, forming a new conducting boundary layer at its roof. Evidence for such an event is recorded in sample GT3A-98Z-2, 32–37 cm, where a dike–gabbro contact was overprinted to microcrystalline hornfels (Fig. 5; see Sect. 5.2).

6 Conclusion

Gabbros in the OmanDP drill core GT3A from the Wadi Abdah of the Oman ophiolite can be regarded as the magmatic outcome of a dynamic axial melt lens horizon and its episodic upward and downward movement. In situ crystallization is the dominant magmatic process, forming early poikilitic clusters followed by the crystallization of the intergranular melt to a granular network under conditions of disequilibrium, as expressed by the marked zoning of the minerals in the gabbros. In contrast to EPR gabbros, the dominance of magmatic amphibole together with the absence of orthopyroxene and the generally higher An contents in plagioclase indicate high water activities in the parental melts feeding the Oman paleocrust. Thermodynamic modeling reveals initial water contents of 0.2 wt %–0.8 wt % in the parental melts feeding the main part of the crust of the Oman ophiolite, in accord with other estimations of initial water content. While the evolved gabbros of our sample set (oxide gabbros) could be regarded as frozen melts, the majority of the gabbros (olivine-bearing gabbros and gabbros) show a distinct cumulate character. The drill core GT3A enables a deep insight into 400 m of the dike–gabbro transition of typical fast-spreading crust, revealing highly complex dike–gabbro contact relationships. Characteristic are varitextured gabbros intruding/stoping earlier previously altered sheeted dikes and basaltic dikes cutting through earlier gabbros. This highlights the activity of a highly dynamic AML, characterized by changing conditions in the transition between the magmatic and metamorphic regime.

Data availability. The Supplement with data related to this article, including Fig. S1 and Tables S1–S3, is available online through the

link provided below or via the "Download & links" section of the article on the *European Journal of Mineralogy* website.

Supplement. The supplement related to this article is available online at: https://doi.org/10.5194/ejm-34-603-2022-supplement.

Author contributions. AE created all the figures and diagrams. AE also wrote the manuscript and took the lead in doing so. The manuscript received support from JK for the first major revisions and from APJ for the second major revisions. Furthermore, JK helped supervise the project from which the research article has been established. CZ provided information on the MELTS modeling, and AE carried out all the modeling and finalized it in the corresponding diagram. DGS performed the bulk rock analysis.

Competing interests. The contact author has declared that none of the authors has any competing interests.

Disclaimer. Publisher's note: Copernicus Publications remains neutral with regard to jurisdictional claims in published maps and institutional affiliations.

Acknowledgements. We are grateful for the careful preparation of samples by Julian Feige. We thank the reviewers Hugh Rollinson and Carlotta Ferrando, as well as editor Riccardo Tribuzio, for their helpful comments and suggestions that substantially improved this paper. We want to thank Ashley Martin for their support on improving this paper.

This research used samples and/or data provided by the Oman Drilling Project. The Oman Drilling Project (OmanDP) has been possible through co-mingled funds from the International Continental Scientific Drilling Project (ICDP; Peter B. Kelemen, Jürg M. Matter, Damon A. H. Teagle lead PIs), the Sloan Foundation – Deep Carbon Observatory (grant 2014-3-01, Peter B. Kelemen PI), the National Science Foundation (NSF-EAR-1516300, Peter B. Kelemen lead PI), NASA Astrobiology Institute (NNA15BB02A, Alexis Templeton PI), the German Research Foundation (DFG; KO 1723/21-1, Jürgen Koepke PI), the Japan Society for the Promotion of Science (JSPS; no. 16H06347, Katsuyoshi Michibayashi PI, and KAKENHI 16H02742, Eiichi Takazawa PI), the European Research Council (Adv: no. 669972, Bjørn Jamveit PI), the Swiss National Science Foundation (SNF; 20FI21_163073, Gretchen Früh-Green PI), JAMSTEC, and the TAMU JR Science Operator and contributions from the Sultanate of Oman Ministry of Regional Municipalities and Water Resources, the Oman Public Authority for Mining, Sultan Qaboos University, CNRS Univ. Montpellier, Columbia University in the City of New York, and the University of Southampton. This study was funded by DFG projects KO 1723/26. Ana Patrícia Jesus acknowledges the Horizon 2020 research and innovation program under the Marie Sklodowska-Curie grant agreement no. 894599.

Financial support. This research has been supported by the Deutsche Forschungsgemeinschaft (DFG; KO 1723/21-1 and KO 1723/26-1).

The publication of this article was funded by the open-access fund of Leibniz Universität Hannover.

Review statement. This paper was edited by Riccardo Tribuzio and reviewed by Hugh Rollinson and Carlotta Ferrando.

References

Alt, J. C., Laverne, C., Coggon, R. M., Teagle, D. A. H., Banerjee, N. R., Morgan, S., Smith-Duque, C. E., Harris, M., and Galli, L.: Subsurface structure of a submarine hydrothermal system in ocean crust formed at the East Pacific Rise, ODP/IODP Site 1256, Geochem. Geophy. Geosy., 11, Q10010, https://doi.org/10.1029/2010GC003144, 2010.

Bédard, J. H.: A procedure for calculating the equilibrium distribution of trace elements among the minerals of cumulate rocks, and the concentration of trace elements in the coexisting liquids, Chem. Geol., 118, 143–153, https://doi.org/10.1016/0009-2541(94)90173-2, 1994.

Bédard, J. H., Sparks, R. S. J., Renner, R., Cheadle, M. J., and Hallworth, M. A.: Peridotite Sills and Metasomatic Gabbros in the Eastern Layered Series of the Rhum Complex, J. Geol. Soc., 145, 207–224, 1988.

Belgrano, T. M. and Diamond, L. W.: Subduction-zone contributions to axial volcanism in the Oman–UAE ophiolite, Lithosphere, 11, 399–411, https://doi.org/10.1130/L1045.1, 2019.

Belgrano, T. M., Diamond, L. W., Vogt, Y., Biedermann, A. R., Gilgen, S. A., and Al-Tobi, K.: A revised map of volcanic units in the Oman ophiolite: insights into the architecture of an oceanic proto-arc volcanic sequence, Solid Earth, 10, 1181–1217, https://doi.org/10.5194/se-10-1181-2019, 2019.

Bosch, D., Jamais, M., Boudier, F., Nicolas, A., Dautria, J.-M., and Agrinier, P.: Deep and high-temperature hydrothermal circulation in the Oman ophiolite – Petrological and isotopic evidence, J. Petrol., 45, 1181–1208, 2004.

Botcharnikov, R., Koepke, J., Holtz, F., McCammon, C., and Wilke, M.: The effect of water activity on the oxidation and structural state of Fe in a ferro-basaltic melt, Geochim. Cosmochim. Ac., 69, 5071–5085, https://doi.org/10.1016/j.gca.2005.04.023, 2005.

Boudier, F., Nicolas, A., and Ildefonse, B.: Magma chambers in the Oman ophiolite: Fed from the top and the bottom, Earth Planet. Sc. Lett., 144, 239–250, 1996.

Canales, J. P., Detrick, R. S., Toomey, D. R., and Wilcock, W. S. D.: Segment-scale variations in the crustal structure of 150–300 kyr old fast spreading oceanic crust (East Pacific Rise, 8 degrees 15′ N-10 degrees 5′ N) from wide-angle seismic refraction profiles, Geophys. J. Int., 152, 766–794, 2003.

Coogan, L. A., Wilson, R. N., Gillis, K. M., and MacLeod, C. J.: Near-solidus evolution of oceanic gabbros: Insights from amphibole geochemistry, Geochim. Cosmochim. Ac., 65, 4339–4357, 2001.

Coogan, L. A., Thompson, G., and MacLeod, C. J.: A textural and geochemical investigation of high level gabbros from the Oman ophiolite: implications for the role of the axial magma chamber at fast-spreading ridges, Lithos, 63, 67–82, 2002.

Coogan, L. A., Mitchell, N. C., and O'Hara, M. J.: Roof assimilation at fast spreading ridges: An investigation combining geophysical, geochemical, and field evidence, J. Geophys. Res.-Sol. Ea., 108, 2002, https://doi.org/10.1029/2001JB001171, 2003.

Cravinho, A., Jesus, A. P., Moreira B., Mateus, A., Pracejus, B. P., Figueiras, J., Benoit, M., Bauer, W., and Rocha, F.: Contrasting features and volcanostratigraphy of the mafic hosted Mandoos ans Shinas VMS Deposits, Samail Ophiolite, Oman, Econ. Geol., accepted, 2022.

Currin, A., Koepke, J., Almeev, R., and Beermann, O.: Interaction of highly saline fluid and olivine gabbro: experimental simulation of deep hydrothermal processes involving amphibole at the base of the oceanic crust, Lithos, 323, 91–102, 2018a.

Currin, A., Wolff, E. P., Koepke, J., Almeev, R., Zhang, C., Zihlmann, B., Ildefonse, B., and Teagle, D. A. H.: Chlorine-rich amphibole in deep layered gabbros as evidence for brine/rock interaction in the lower oceanic crust: a case study from the Wadi Wariyah, Samail Ophiolite, Sultanate of Oman, Lithos, 323, 125–136, 2018b.

De Graaff, S. J., Goodenough, K., Klaver, M., Lissenberg, C., Jansen, M., Millar, I., and Davies, G.: Evidence for a moist to wet source transition throughout the Oman-UAE ophiolite, and implications for the geodynamic history, Geochem. Geophy. Geosy., 20, 651–672, https://doi.org/10.1029/2018GC007923, 2019.

Detrick, R. S., Buhl, P., Vera, E., Mutter, J., Orcutt, J., Madsen, J., and Brocher, T.: Multichannel seismic imaging of a crustal magma chamber along the East Pacific Rise, Nature, 326, 35–41, 1987.

Erdmann, M., France, L., Fischer, L. A., Deloule, E., and Koepke, J.: Trace elements in anatectic products at the roof of mid-ocean ridge magma chambers: An experimental study, Chem. Geol., 456, 43–57, https://doi.org/10.1016/j.chemgeo.2017.03.004, 2017.

Ernst, W. G. and Liu, J.: Experimental phase-equilibrium study of Al- and Ti-contents of calcic amphibole in MORB – a semiquantitative thermobarometer, Am. Mineral., 83, 952–969, 1998.

Feig, S., Koepke, J., and Snow, J.: Effect of water on tholeiitic basalt phase equilibria: An experimental study under oxidizing conditions, Contrib. Mineral. Petr., 152, 611–638, 2006.

Fischer, L. A., Erdmann, M., France, L., Wolff, P. E., Deloule, E., Zhang, C., Godard, M., and Koepke, J.: Trace element evidence for anatexis at oceanic magma chamber roofs and the role of partial melts for contamination of fresh MORB, Lithos, 260, 1–8, https://doi.org/10.1016/j.lithos.2016.05.001, 2016.

France, L.: Magmatic/hydrothermal interactions at fast spreading mid-ocean ridges: implications on the dynamics of the axial melt lens, PhD thesis, Univ. Montpellier, 2009.

France, L., Ildefonse, B., and Koepke, J.: Interactions between magma and the hydrothermal system in the Oman ophiolite and in IODP hole 1256D: fossilisation of a dynamic melt lens at fast spreading ridges, Geochem. Geophy. Geosy., 10, Q10O19, https://doi.org/10.1029/2009GC002652, 2009.

France, L., Koepke, J., Ildefonse, B., Cichy, S., and Deschamps, F.: Hydrous partial melting in the sheeted dike complex at fast spreading ridges: experimental and natural observations, Contrib. Mineral. Petr., 159, 683–704, https://doi.org/10.1007/s00410-010-0502-6, 2010.

France, L., Ildefonse, B., and Koepke, J.: Hydrous magmatism triggered by assimilation of hydrothermally altered rocks in fossil oceanic crust (northern Oman ophiolite), Geochem. Geophy. Geosy., 14, 2598–2614, https://doi.org/10.1002/ggge.20137, 2013.

France, L., Lombard, M., Nicollet, C., Berthod, C., Debret, B., Koepke, J., Ildefonse, B., and Toussaint, A.: Quantifying the axial magma lens dynamics at the roof of oceanic magma reservoirs (dike/gabbro transition): Oman Drilling Project GT3 site survey, J. Geophys. Res.-Sol. Ea., 126, e2020JB021496, https://doi.org/10.1029/2020JB021496, 2021.

Fricker, M. B., Kutscher, D., Aeschlimann, B., Frommer, J., Dietiker, R., Bettmer, J., and Günther, D.: High spatial resolution trace element analysis by LA-ICP-MS using a novel ablation cell for multiple or large samples, Int. J. Mass Spectrom., 307, 39–45, 2011.

Gaetani, G. A., Grove, T. L., and Bryan, W. B.: The influence of water on the petrogenesis of subduction related igneous rocks, Nature, 365, 332–334, https://doi.org/10.1038/365332a0, 1993.

Gale, A., Dalton, C. A., Langmuir, C. H., Su, Y., and Schiling, J.: The mean composition of ocean ridge basalts, Geochem. Geophy. Geosy., 14, 489–518, https://doi.org/10.1029/2012GC004334, 2013.

Garbe-Schönberg, D.: Simultaneous determination of thirty-seven trace elements in twenty-eight international rock standards by ICP-MS, Geostandard. Newslett., 17, 81–97, https://doi.org/10.1111/j.1751-908X.1993.tb00122.x, 1993.

Garbe-Schönberg, D. and Müller, S.: Nano-particulate pressed powder tablets for LA-ICP-MS, J. Anal. Atom. Spectrom., 29, 990–1000, https://doi.org/10.1039/C4JA00007B, 2014.

Garbe-Schönberg, D., Koepke, J., Müller, S., Mock, D., and Müller, T.: A reference section through fast-spread lower oceanic crust, Wadi Gideah, Samail Ophiolite (Sultanate of Oman): whole rock geochemistry, J. Geophys. Res.-Sol. Ea., 127, e2021JB022734, https://doi.org/10.1029/2021JB022734, 2022.

Ghiorso, M. S. and Sack, R. O.: Chemical mass transfer in magmatic processes. IV. A revised and internally consistent thermodynamic model for the interpolation and extrapolation of liquid-solid equilibria in magmatic systems at elevated temperatures and pressures, Contrib. Mineral. Petr., 84, 107–145, 1995.

Gillis, K. M. and Meyer, P. S.: Metasomatism of oceanic gabbros by late stage melts and hydrothermal fluids: Evidence from the rare earth element composition of amphiboles, Geochem. Geophy. Geosy., 2, 2000GC000087, https://doi.org/10.1029/2000GC000087, 2001.

Gillis, K. M., Coogan, L. A., and Chaussidon, M.: Volatile element (B, Cl, F) behaviour in the roof of an axial magma chamber from the East Pacific Rise, Earth Planet. Sc. Lett., 213, 447–462, 2003.

Godard, M., Dautria, J.-M., and Perrin, M.: Geochemical variability of the Oman ophiolite lavas: Relationship with spatial distribution and paleomagnetic directions, Geochem. Geophy. Geosy., 4, 2002GC000452, https://doi.org/10.1029/2002GC000452, 2003.

Goodenough, K. M., Thomas, R. J., Styles, M. T., Schofield, D. I., and MacLeod, C. J.: Records of Ocean Growth and Destruction in the Oman-UAE Ophiolite, Elements, 10, 109–114, https://doi.org/10.2113/gselements.10.2.109, 2014.

Govindaraju, K.: 1995 working values with confidence limits for twenty-six CRPG, ANRT and IWG-GIT geostandards, Geostandard. Newslett., 19, 1–32, https://doi.org/10.1111/j.1751-908X.1995.tb00164.x, 1995.

Guilmette, C., Smit, M. A., van Hinsbergen, D. J., Gürer, D., Corfu, F., Charette, B., Maffione, M., Rabeau, O., and Savard, D.: Forced subduction initiation recorded in the sole and crust of the Semail Ophiolite of Oman, Nat. Geosci., 11, 688–695, https://doi.org/10.1038/s41561-018-0209-2, 2018.

Hawthorne, F. C., Oberti, R., Harlow, G. E., Maresch, W. V., Martin, R. F., Schumacher, J. C., and Welch, M. D.: Nomenclature of the amphibole supergroup, Am. Mineral., 97, 2031–2048, https://doi.org/10.2138/am.2012.4276, 2012.

Henstock, T. J., Woods, A. W., and White, R. S.: The accretion of oceanic crust by episodic sill intrusion, J. Geophys. Res.-Sol. Ea., 98, 4143–4161, 1993.

Holland, T. J. B. and Blundy, J.: Non-ideal Interactions in calcic amphiboles and their bearing on amphibole-plagioclase thermometry, Contrib. Mineral. Petr., 116, 433–447, 1994.

Imai, N., Terashima, S., Itoh, S., and Ando, A.: 1994 compilation of analytical data for minor and trace elements in seventeen GSJ geochemical reference samples,"Igneous rock series", Geostandard. Newslett., 19, 135–213, https://doi.org/10.1111/j.1751-908X.1995.tb00158.x, 1995.

Jochum, K. P. and Jenner, G.: Trace element analysis of Geological Survey of Japan silicate reference materials: comparison of SSMS with ICP-MS data and a critical discussion of compiled values, Fresen. J. Anal. Chem., 350, 310–318, 1994.

Jochum, K. P., Weis, U., Schwagner, B., Stoll, B., Wilson, S. A., Haug, G. H., and Enzweiler, J.: Reference values following ISO guidelines for frequently requested rock reference materials, Geostand. Geoanal. Res., 40, 333–350, https://doi.org/10.1111/j.1751-908X.2015.00392.x, 2016.

Juteau, T., Beurrier, M., Dahl, R., and Nehlig, P.: Segmentation at a fossil spreading axis: The plutonic sequence of the Wadi Haymiliyah area (Haylayn Block, Sumail Nappe, Oman), Tectonophysics, 151, 167–197, 1988.

Kelemen, P. B., Koga, K., and Shimizu, N.: Geochemistry of gabbro sills in the crust-mantle transition zone of the Oman ophiolite: Implications for the origin of the oceanic lower crust, Earth Planet. Sc. Lett., 146, 475–488, 1997.

Kelemen, P. B., Matter, J. M., Teagle, D. A. H., Coggon, J. A., and the_Oman_Drilling_Project_Science_Team: Site GT3: sheeted dike to gabbro transition, Proceedings of the Oman Drilling Project, College Station, TX (International Ocean Discovery Program), https://doi.org/10.14379/OmanDP.proc.2020, 2020.

Kendrick, M. A.: Halogens in altered ocean crust from the East Pacific Rise (ODP/IODP Hole 1256D), Geochim. Cosmochim. Ac., 261, 93–112, https://doi.org/10.1016/j.gca.2019.06.044, 2019.

Kinzler, R. J. and Grove, T. L.: Corrections and further discussion of the primary magmas of midocean ridge basalts, 1 and 2, J. Geophys. Res.-Sol. Ea., 98, 22339–22347, https://doi.org/10.1029/93jb02164, 1993.

Koepke, J. and Zhang, C.: Axial Melt-Lens Dynamics at Fast Spreading Midocean Ridges, in: Dynamic magma evolution, edited by: Vetere, F., American Geophysical Union, 179–206, https://doi.org/10.1002/9781119521143.ch9, 2020.

Koepke, J., Berndt, J., and Bussy, F.: An experimental study on the shallow-level migmatization of ferrogabbros from the Fuerteventura Basal Complex, Canary islands, Lithos, 69, 105–125, https://doi.org/10.1016/S0024-4937(03)00049-5, 2003.

Koepke, J., Feig, S. T., and Snow, J.: Late stage magmatic evolution of oceanic gabbros as a result of hydrous partial melting: Evidence from the Ocean Drilling Program (ODP) Leg 153 drilling at the Mid-Atlantic Ridge, Geochem. Geophy. Geosy., 6, Q02001, https://doi.org/10.1029/2004GC000805, 2005.

Koepke, J., Christie, D. M., Dziony, W., Holtz, F., Lattard, D., Maclennan, J., Park, S., Scheibner, B., Yamasaki, T., and Yamasaki, S.: Petrography of the Dike/Gabbro Transition at IODP Site 1256D (Equatorial Pacific): The evolution of the Granoblastic Dikes, Geochem. Geophy. Geosy., 9, Q07O09, https://doi.org/10.1029/2008GC001939, 2008.

Koepke, J., France, L., Müller, T., Faure, F., Goetze, N., Dziony, W., and Ildefonse, B.: Gabbros from IODP Site 1256 (Equatorial Pacific): Insight into axial magma chamber processes at fast-spreading ocean ridges Geochem. Geophy. Geosy., 12, Q09014, https://doi.org/10.1029/2011GC003655, 2011.

Koepke, J., Botcharnikov, R. E., and Natland, J. H.: Crystallization of late-stage MORB under varying water activities and redox conditions: Implications for the formation of highly evolved lavas and oxide gabbro in the ocean crust, Lithos, 323, 58–77, https://doi.org/10.1016/j.lithos.2018.10.001, 2018.

Koepke, J., Feig, S., Berndt, J., and Neave, D.: Wet magmatic processes during the accretion of the deep crust of the Oman Ophiolite paleoridge: Phase diagrams and petrological records, Tectonophysics, 817, 229051, https://doi.org/10.1016/j.tecto.2021.229051, 2021.

Koepke, J., Garbe-Schönberg, D., Müller, T., Mock, D., Müller, S., and Nasir, S.: A Reference Section Through Fast-Spread Lower Oceanic Crust, Wadi Gideah, Samail Ophiolite (Sultanate of Oman): Petrography and Petrology, J. Geophys. Res.-Sol. Ea., 127, e2021JB022735, https://doi.org/10.1029/2021JB022735, 2022.

Le Bas, M. J. and Streckeisen, A.: The IUGS systematics of igneous rocks, J. Geol. Soc., 148, 825–833, https://doi.org/10.1144/gsjgs.148.5.0825, 1991.

Locock, A. J.: An Excel spreadsheet to classify chemical analyses of amphiboles following the IMA 2012 recommendations, Comput. Geosci., 62, 1–11, 2014.

MacLeod, C. J. and Yaouancq, G.: A fossil melt lens in the Oman ophiolite: Implications for magma chamber processes at fast spreading ridges, Earth Planet. Sc. Lett., 176, 357–373, 2000.

MacLeod, C. J., Lissenberg, C. J., and Bibby, L. E.: "Moist MORB" axial magmatism in the Oman ophiolite: The evidence against a mid-ocean ridge origin, Geology, 41, 459–462, https://doi.org/10.1130/g33904.1, 2013.

Maher, S. M., Gee, J. S., Cheadle, M. J., and John, B. E.: Three-dimensional magnetic stripes require slow cooling in fast-spread lower ocean crust, Nature, 597, 511–515, https://doi.org/10.1038/s41586-021-03831-6, 2021.

Manning, C. and Aranovich, L.: Brines at high pressure and temperature: thermodynamic, petrologic and geochemical effects, Precambrian Res., 253, 6–16, https://doi.org/10.1016/j.precamres.2014.06.025, 2014.

Manning, C. E., MacLeod, C. J., and Weston, P. E.: Lower-crustal cracking front at fast-spreading ridges: Evidence from the East Pacific Rise and the Oman ophiolite, in: Ophiolites and oceanic crust: New insights from field studies and the Ocean Drilling

Program, edited by: Dilek, Y., Moores, E. M., Elthon, D., and Nicolas, A., Geological Society of America Special Paper 349, Boulder, Colorado, 261–272, ISBN 0-8137-2349-3, 2000.

Michael, P. J. and Schilling, J.-G.: Chlorine in mid-ocean ridge magmas: evidence for assimilation of seawater-influenced components, Geochim. Cosmochim. Ac., 53, 3131–3143, https://doi.org/10.1016/0016-7037(89)90094-X, 1989.

Mock, D., Ildefonse, B., Müller, T., and Koepke, J.: A reference section through fast-spread lower oceanic crust, Wadi Gideah, Samail Ophiolite (Sultanate of Oman): Insights from Crystallographic Preferred Orientations, J. Geophys. Res.-Sol. Ea., 126, e2021JB021864, https://doi.org/10.1029/2021JB021864, 2021.

Morgan, J. P. and Chen, Y. J.: The genesis of oceanic crust: Magma injection, hydrothermal circulation, and crustal flow, J. Geophys. Res.-Sol. Ea., 98, 6283–6297, 1993.

Müller, T.: A petrological and geochemical cross section of lower crust at the Wadi Gideah (Samail ophiolite): Implications for the crustal accretion at fast-spreading mid-ocean ridges, PhD, University of Hannover, 199 pp., 2016.

Müller, T., Koepke, J., Garbe-Schönberg, C. D., Dietrich, M., Bauer, U., and Wolff, P. B.: Anatomy of a frozen axial melt lens from a fast-spreading paleo-ridge (Wadi Gideah, Oman ophiolite), Lithos, 272, 31–45, https://doi.org/10.1016/j.lithos.2016.11.022, 2017.

Natland, J. H. and Dick, H. J. B.: Paired melt lenses at the East Pacific Rise and the pattern of melt flow through the gabbroic layer at a fast-spreading ridge, Lithos, 112, 73–86, 2009.

Neo, N., Yamazaki, S., and Miyashita, S.: Data report: Bulk rock compositions of samples from the IODP Expedition 309/312 sample pool, ODP Hole 1256D, in: Proc. IODP, Sci. Results, 309/312, edited by: Teagle, D. A. H., Alt, J. C., Umino, S., Miyashita, S., Banerjee, N. R., and Wilson, D. S., College Station, TX, Ocean Drilling Program, https://doi.org/10.2204/iodp.proc.309312.204.2009, 2009.

Nicolas, A. and Boudier, F.: Large mantle upwellings and related variations in crustal thickness in the Oman ophiolite, Geol. S. Am. S., 349, 67–74, https://doi.org/10.1130/0-8137-2349-3.67, 2000.

Nicolas, A., Boudier, F., Koepke, J., France, L., Ildefonse, B., and Mevel, C.: Root zone of the sheeted dike complex in the Oman ophiolite, Geochem. Geophy. Geosy., 9, Q05001, https://doi.org/10.1029/2007GC001918, 2008.

Pichavant, M. and Macdonald, R.: Crystallization of primitive basaltic magmas at crustal pressures and genesis of the calc-alkaline igneous suite: experimental evidence from St Vincent, Lesser Antilles arc, Contrib. Mineral. Petr., 154, 553–558, https://doi.org/10.1007/s00410-007-0208-6, 2007.

Pouchou, J. L. and Pichoir, F.: Quantitative analysis of homogeneous or stratified microvolumes applying the model “PAP”, in: Electron probe quantification, edited by: Heinrich, K. F. J. and Newbury, D. E., Plenum Press, New York, 31–75, https://doi.org/10.1007/978-1-4899-2617-3_4, 1991.

Quick, J. E. and Denlinger, R. P.: Ductile deformation and the origin of layered gabbro in ophiolites, J. Geophys. Res.-Sol. Ea., 98, 14015–14027, 1993.

Rioux, M., Bowring, S., Kelemen, P., Gordon, S., Dudas, F., and Miller, R.: Rapid crustal accretion and magma assimilation in the Oman-UAE ophiolite: High precision U-Pb zircon geochronology of the gabbroic crust, J. Geophys. Res.-Sol. Ea., 117, https://doi.org/10.1029/2012jb009273, 2012.

Rioux, M., Bowring, S., Kelemen, P., Gordon, S., Miller, R., and Dudas, F.: Tectonic development of the Samail ophiolite: High-precision U-Pb zircon geochronology and Sm-Nd isotopic constraints on crustal growth and emplacement, J. Geophys. Res.-Sol. Ea., 118, 2085–2101, https://doi.org/10.1002/jgrb.50139, 2013.

Rioux, M., Garber, J. M., Searle, M., Kelemen, P., Miyashita, S., Adachi, Y., and Bowring, S.: High-precision U-Pb zircon dating of late magmatism in the Samail ophiolite: A record of subduction initiation, J. Geophys. Res.-Sol.Ea., 126, https://doi.org/10.1029/2020JB020758, 2021.

Rollinson, H.: Using geochemical data. Evaluation, presentation, interpretation, 2nd Edn., Cambridge University Press, https://doi.org/10.1017/9781108777834, 1993.

Sato, H., Holtz, F., Behrens, H., Botcharnikov, R., and Nakada, S.: Experimental petrology of the 1991–1995 Unzen dacite, Japan. Part II: Cl/OH partitioning between hornblende and melt and its implications for the origin of oscillatory zoning of hornblende phenocrysts, J. Petrol., 46, 339–354, https://doi.org/10.1093/petrology/egh078, 2005.

Sinton, J. M. and Detrick, R. S.: Midocean ridge magma chambers, J. Geophys. Res.-Sol. Ea., 97, 197–216, 1992.

Staudigel, H.: Hydrothermal alteration processes in the oceanic crust, Treatise on geochemistry, 3, 659, https://doi.org/10.1016/B0-08-043751-6/03032-2, 2003.

Teagle, D. A., Ildefonse, B., and Blum, P.: IODP expedition 335: Deep sampling in ODP hole 1256D, Scientific Drilling, 13, 28–34, https://doi.org/10.2204/iodp.sd.13.04.2011, 2012.

Toplis, M. J. and Carroll, M. R.: An experimental study of the influence of oxygen fugacity on Fe-Ti oxide stability, phase relations, and mineral-melt equilibra in ferro-basaltic systems, J. Petrol., 36, 1137–1170, https://doi.org/10.1093/petrology/36.5.1137, 1995.

Tribuzio, R., Tiepelo, M., and Thirlwall, M. F.: Origin of titanian pargasite in gabbroic rocks from the Northern Apennine ophiolites (Italy): insights into the late-magmatic evolution of a MOR-type intrusive sequence, Earth Planet. Sc. Lett., 176, 281–293, https://doi.org/10.1016/S0012-821X(00)00014-5, 2000.

VanTongeren, J., Kelemen, P., Garrido, C., Godard, M., Hanghoj, K., Braun, M., and Pearce, J.: The composition of the lower oceanic crust in the Wadi Khafifah section of the southern Samail (Oman) ophiolite, J. Geophys. Res.-Sol. Ea., 126, e2021JB021986, https://doi.org/10.1029/2021JB021986, 2021.

Vera, E. E., Mutter, J. C., Buhl, P., Orcutt, J. A., Harding, A. J., Kappus, M. E., Detrick, R. S., and Brocher, T. M.: The structure of 0-my to 0.2-my old oceanic crust at 9° N on the East Pacific Rise from expanded spread profiles, J. Geophys. Res.-Solid, 95, 15529–15556, https://doi.org/10.1029/JB095iB10p15529, 1990.

Wanless, V. D. and Shaw, A. M.: Lower crustal crystallization and melt evolution at mid-ocean ridges, Nat. Geosci., 5, 651–655, https://doi.org/10.1038/NGEO1552, 2012.

Wolff, P. E., Koepke, J., and Feig, S. T.: The reaction mechanism of fluid-induced partial melting of gabbro in the oceanic crust, Eur. J. Mineral., 25, 279–298, https://doi.org/10.1127/0935-1221/2013/0025-2314, 2013.

Zhang, C., Koepke, J., Kirchner, C., Gotze, N., and Behrens, H.: Rapid hydrothermal cooling above the axial melt lens at fast-spreading mid-ocean ridge, Sci. Rep.-UK, 4, 6342, https://doi.org/10.1038/srep06342, 2014.

Zhang, C., Koepke, J., France, L., and Godard, M.: Felsic Plutonic Rocks from IODP Hole 1256D, Eastern Pacific: Implications for the Nature of the Axial Melt Lens at Fast-Spreading Mid-Ocean Ridges, J. Petrol., 58, 1535–1565, https://doi.org/10.1093/petrology/egx064, 2017.

Zhang, C., Koepke, J., Wolff, P. E., Horn, I., Garbe-Schönberg, D., and Berndt, J.: Multi-stage Hydrothermal Veins in Layered Gabbro of the Oman Ophiolite: Implications for Focussed Fluid Circulation in the Lower Oceanic Crust, J. Geophys. Res.-Sol. Ea., 126, e2021JB022349, https://doi.org/10.1029/2021JB022349, 2021.

Zihlmann, B., Müller, S., Coggon, R. M., Koepke, J., Garbe-Schönberg, D., and Teagle, D. A.: Hydrothermal fault zones in the lower oceanic crust: An example from Wadi Gideah, Samail ophiolite, Oman, Lithos, 323, 103–124, https://doi.org/10.1016/j.lithos.2018.09.008, 2018.